Quaternary Science Reviews 250 (2020) 106679

Contents lists available at ScienceDirect

Quaternary Science Reviews

journal homepage: www.elsevier.com/locate/quascirev

Ecological response of a glacier-fed peatland to late Holocene climate and glacier changes on subantarctic South Georgia

Zhengyu Xia [a, *, 1], Lea Toska Oppedal [b], Nathalie Van der Putten [c], Jostein Bakke [b], Zicheng Yu [a, d]

[a] Department of Earth and Environmental Sciences, Lehigh University, Bethlehem, PA, USA
[b] Department of Earth Science and Bjerknes Centre for Climate Research, University of Bergen, Bergen, Norway
[c] Department of Earth Sciences, Vrije Universiteit Amsterdam, Amsterdam, the Netherlands
[d] Institute for Peat and Mire Research, School of Geographical Sciences, Northeast Normal University, Changchun, China

ARTICLE INFO

Article history:
Received 10 July 2020
Received in revised form
24 October 2020
Accepted 25 October 2020
Available online 7 November 2020

Keywords:
South Georgia
Late Holocene
Glaciers
Peatlands
Meltwater
Brown mosses
Stable isotopes

ABSTRACT

Sedimentary deposits from glacier-fed peatlands provide records of past glacier variability, but the dynamics of these peat-forming ecosystems have rarely been investigated. Through multi-proxy analyses of a 204-cm peat core, we reconstructed the ecological response of a glacier-fed peatland on subantarctic South Georgia to climate and glacier variability over the last 4300 years. A stable peatland with rapid carbon accumulations and dynamic turnovers between brown mosses and monocots persisted between 4300 and 2550 cal yr BP when the up-valley cirque glacier was small under a regional hypsithermal climate. Carbon accumulation rates showed two peak periods driven by climate warming, reaching 140 g C m^{-2} yr^{-1} at 4000–3500 cal yr BP and 70 g C m^{-2} yr^{-1} at 3200–2700 cal yr BP. Paired $\delta^{13}C$ and $\delta^{18}O$ data from brown moss cellulose reveal several intervals of glacial meltwater inundation that caused short-term disturbances of the peatland vegetation, indicating that glacial meltwater potentially still affected the peatland ecosystem during this warm period. Moss-dominated vegetation was disrupted and peatland carbon accumulation rates decreased to 15 g C m^{-2} yr^{-1} after around 2550 cal yr BP when a cooling-driven glacier advance shifted the erosion and meltwater regime enhancing the glacial sediment influx onto the peatland. Although this enhanced regime of meltwater disturbance has continued since this transition, the brown moss habitat was gradually re-established during the medieval climate warming between 1200 and 600 cal yr BP and then became dominant shortly after that. This re-establishment of brown mosses might have benefited from a period of increased carbon accumulation rates up to 100 g C m^{-2} yr^{-1} at 1200–900 cal yr BP that built up the organic matter matrix and stabilized the habitat. We conclude that the ecosystem dynamics of glacier-fed peatlands is strongly shaped by the interplay between regional climate and glacier activity. This study also demonstrates the potential of stable isotope analysis in studying the paleohydrology of non-*Sphagnum* peatlands.

1. Introduction

The mass balance and extent of glaciers are sensitive to climate change. Reconstructions of past glacier fluctuations therefore provide indirect but often robust records of long-term climate variability beyond the instrumental period. Mapping and dating of glacial moraines is a common approach to reconstruct the timing and extent of past glaciations (Owen et al., 2005; Bentley et al., 2007; Schaefer et al., 2009). Another approach is to utilize the record of glacially eroded sediments, dominated by clay and silt particles, transported by glacial meltwater and preserved in downstream locations, as a continuous archive for upstream glacier variability. This approach has been used in glacier-fed lake sediment (glaciolacustrine) records and could be combined with glacial moraine evidence to quantify the long-term variations in the equilibrium-line-altitude of glaciers (Dahl et al., 2003; Daigle and Kaufman, 2009; Bakke et al., 2010; Røthe et al., 2015).

Glacier-fed peatlands could also provide continuous and high-resolution records of glacier activity. These peatlands are subject

* Corresponding author.
E-mail address: zhengyuxia@umass.edu (Z. Xia).
[1] Present address: Department of Geosciences, University of Massachusetts Amherst, Amherst, MA 01003–9297, USA.

https://doi.org/10.1016/j.quascirev.2020.106679
0277-3791/

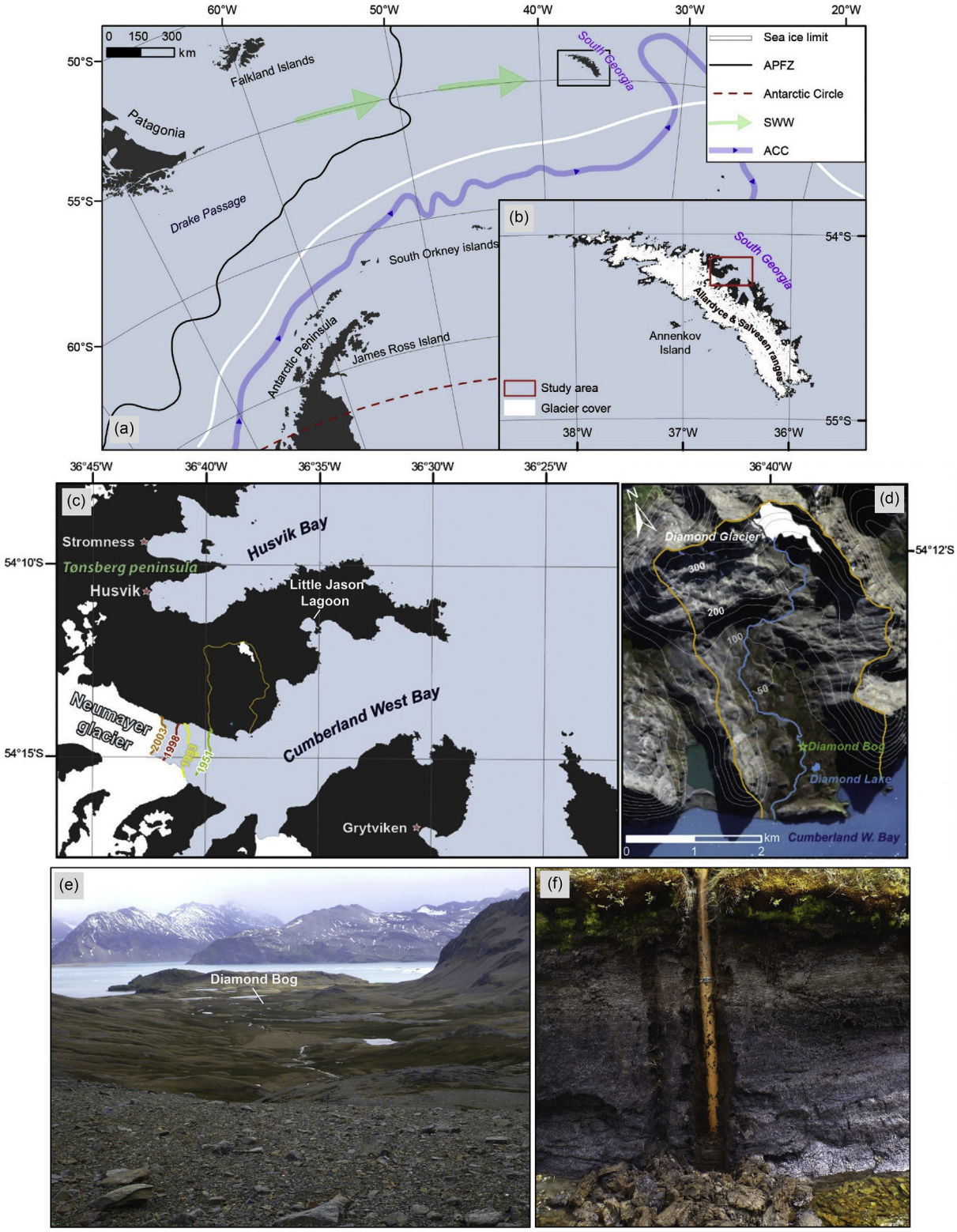

Fig. 1. Regional and local setting for Diamond Bog. (a) Overview map showing South Georgia in the southern Atlantic Ocean. Also shown are the Antarctic Polar Front Zone (APFZ), the Southern Westerly Winds (SWW), the Antarctic Circumpolar Current (ACC), the Antarctic Circle, and the winter sea ice limit. (b) Map of South Georgia main island where our study site Diamond Bog is located and Annenkov Island where Fan Lake is located. (c) Map of the study area corresponding to the red rectangle area in (b) showing the Diamond Glacier catchment (orange lines). Also shown are other names mentioned in the main text, such as Grytviken where a weather station is based, Neumayer Glacier with historical glacier front positions, and Cumberland West Bay. (d) Satellite image of the Diamond Glacier catchment with elevation contour lines (in meter). Also shown are Diamond Glacier (white polygon), the main glacier meltwater stream (blue line), Diamond Bog where the peat core DB2 was collected (green star), and Diamond Lake. (e) Ground photo looking south showing the overview of the Diamond Glacier catchment and Diamond Bog. (f) Photo of the stream-cut bank at Diamond Bog where the peat core DB2 was collected. Note that (a)–(d) are after Oppedal et al. (2018a). (e) and (f) were taken by J.B. in December 2011. (For interpretation of the references to colour in this figure legend, the reader is referred to the Web version of this article.)

to episodic flooding from sediment-laden glacial meltwater, by which suspended glacial sediments settle out on the peatland surface, resulting in visible or non-visible minerogenic layers within peat deposits (Matthews et al., 2005). There have been some studies utilizing such glaciofluvial archives from glacier-fed peatlands to reconstruct past episodes of glacier advance and retreat (Nesje and Dahl, 1991a, 1991b; Matthews et al., 2005; Matthews and Dresser, 2008; Oppedal et al., 2018a). These studies consider peatlands in glacierized valleys as passive archives for glacial sediments, but, to our knowledge, there is no study characterizing how complex peat-forming ecosystems themselves respond to climate and glacier changes. Glacier-fed peatlands represent an underutilized archive for understanding the peatland ecosystem processes and carbon cycling dynamics, compared to well-studied rain-fed (ombrotrophic) bogs and groundwater-fed fens (Mauquoy et al., 2002; MacDonald et al., 2006; Yu, 2006; Yu et al., 2009).

Subantarctic South Georgia island in the southern Atlantic Ocean is extensively covered by glaciers (Fig. 1a and b), shows well-preserved glacial landforms (Bentley et al., 2007), glacier-fed lakes (Rosqvist and Schuber, 2003; Oppedal et al., 2018a), and a diversity of peat-forming ecosystems in ice-free areas (Lewis-Smith, 1981; Van der Putten et al., 2012). A number of studies have investigated these paleoenvironmental archives to reconstruct the long-term climate history in South Georgia (Clapperton et al., 1989; Birnie, 1990; Rosqvist and Schuber, 2003; Van der Putten et al., 2004, 2009; Bentley et al., 2007; Berg et al., 2018; Oppedal et al., 2018a), a key region for understanding interhemispheric linkages in global climate change and past variability in the Southern Westerly Winds. One of these studies by Oppedal et al. (2018a) utilized paired glaciolacustrine and glaciofluvial records along with moraine mapping to reconstruct past cirque glacier variability, generating a consistent picture of glacier fluctuations comparable with other studies in South Georgia (Rosqvist and Schuber, 2003; Berg et al., 2018). Here, with additional data, we extend the paleoenvironmental analysis of the glaciofluvial record developed by Oppedal et al. (2018a) to document the peatland ecosystem response to past changes in climate and glacier activity. We place our findings from this study in a broad context for understanding the interactions among regional climate, glacial meltwater, glacial sediment disturbances, peatland ecosystems, and carbon accumulations. Our new analyses not only provide additional constraints on regional climate and glacier history during the late Holocene, but also demonstrate the utility of stable isotope analysis of plant macrofossils to reconstruct the wetland changes from peat archives.

2. Regional setting and study site

South Georgia island (54–55°S, 38–36°W) has an elongated shape with a northwest-southeast orientation and is approximately 170 km long and up to 40 km wide (Fig. 1a and b). It has an axial mountain range across the main island with 19 peaks over 2000 m above sea level (asl) (Bannister and King, 2015). While over a half of South Georgia is covered by permanent snow and ice (Gordon et al., 2008), large ice-free areas are present on the northeastern coast (Fig. 1b), a condition that started to establish since the very beginning of the Holocene (Van der Putten and Verbruggen, 2005; Graham et al., 2017; Oppedal et al., 2018a), and thus has been the target area for many research expeditions. The ice-free area—where glaciation is only limited to small cirque and plateau glaciers—is the result of leeside föhn effects that increase temperature, decrease relative humidity, and limit snowfall under the strong Southern Westerly Winds (Bannister and King, 2015; Oppedal et al., 2018a). South Georgia has an overall cool oceanic climate. Weather station data are available from Grytviken (Fig. 1c) since 1905 CE. Based on data from the Global Historical Climatology Network (GHCN), the mean annual temperature is 1.9 °C and the mean summer (December–February) and winter (June–August) temperatures are 4.8 °C and −1.3 °C, respectively. Compared to the same latitude in Patagonia, South Georgia is 4–5 °C colder as it is situated south of the Antarctic Polar Front Zone (Fig. 1a). The mean annual precipitation from the GHCN station is 1450 mm with more

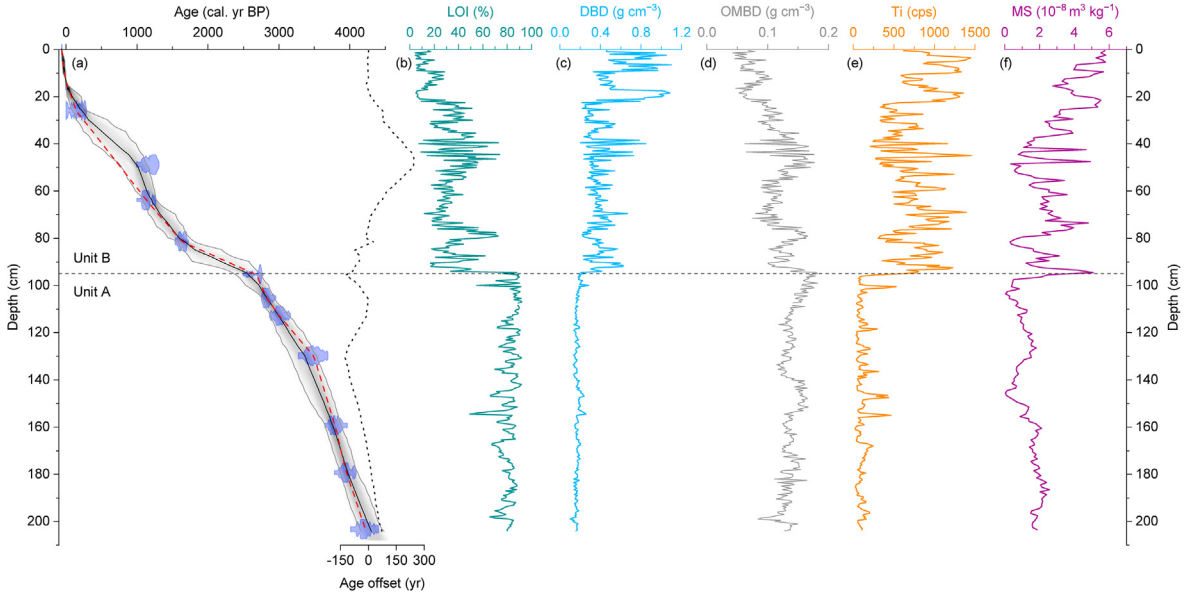

Fig. 2. Summary of existing age and proxy data for the DB2 peat core (Oppedal et al., 2018a). (a) Bacon age-depth model run with default prior information. Also shown is the Clam age-depth model of linear interpolation (dashed red line) after rejecting an outlier at 49 cm (Oppedal et al., 2018a). The median age offset between two age-depth models ("Bacon" age minus "Clam" age) is shown on the right. (b) Loss-on-ignition (LOI). (c) Dry bulk density (DBD). (d) Organic matter bulk density (OMBD) derived by multiplying LOI and DBD data (this study). (e) Titanium (Ti) abundance (counts per second). (f) Mass specific magnetic susceptibility. The dashed horizontal line marks the transition from Unit A to Unit B at 95 cm depth. (For interpretation of the references to colour in this figure legend, the reader is referred to the Web version of this article.)

precipitation in autumn (March–May; 426 mm) and winter (419 mm) than in spring (September–November; 291 mm) and summer (314 mm). Over the last century, weather station data documented a significant trend of increasing temperature of 0.13 °C per decade and increasing precipitation of 45 mm per decade, which became even stronger after 1950 CE (Roberts et al., 2010; Thomas et al., 2018a). The recent warming trend on the north-eastern coast, which has been linked with the recent strengthening of the Southern Westerly Winds and associated föhn events (Bannister and King, 2015; Thomas et al., 2018a), has caused recession of glaciers on South Georgia, especially cirque and small valley glaciers that have a shorter response time (Gordon et al., 2008).

Diamond Glacier is a temperate cirque glacier southwest of the summit of Diamond Peak (510 m asl). Glacier elevations range from 360 to 500 m asl in December 2011 (Fig. 1d), and glacial meltwater drains into Cumberland West Bay through a main channel with a catchment area of 11 km^2 in Olsen Valley (Fig. 1d). The upper valley has exposed bedrocks, unprotected bottom till, numerous moraine ridges and sandbanks, while the lower valley is gently sloping and well vegetated (Fig. 1e). The glacial meltwater follows a well-defined canyon before it reaches the lower valley. Diamond Bog (unofficial name; Oppedal et al., 2018a) is a peatland site in the lower valley. During spring melt, the entire peatland is flooded by glacial meltwater spreading from the root point 2 km up valley. Further down valley, the glacial meltwater stream is meandering in the peatland and the main channel exposes over 2-m peat and minerogenic sediment deposits (Fig. 1f). The field survey indicates that streambanks sometimes collapse and expose fresh peat outcrops (Fig. A1) and also that several incised channels have been active in the past. Further downstream in the main channel, the glacial meltwater regularly drains into Diamond Lake during ablation seasons (Fig. 1d).

Diamond Bog is a soligenous eutrophic peatland, and, according to Lewis-Smith (1981) who defined several peat-forming ecosystems in South Georgia, it is a *Mire Peat* on the basis of the present-day vegetation dominated by the moss *Syntrichia robusta* (syn. *Tortula robusta* Hook. and Grev.), the grass *Festuca contracta*, and the rush including *Rostkovia magellanica* and *Juncus scheuchzeroides/inconspicuous* as well as other vascular plants such as *Acaena magellanica.* The presence of glacial sediments near the peatland surface at the coring site indicates that the site has been subject to flooding from glacial meltwater in recent times.

3. Materials and methods

3.1. Samples

The Diamond Bog peat core (DB2) was collected from an exposed section of the main channel using a PVC tube in December 2011 (Fig. 1f). The core reached bottom till and captured all peat deposits above. The original peat deposit at the site was 220 cm thick, but due to hammering in the PVC tube a compaction of 16 cm was noted in the field, resulting in a 204-cm long peat core. Compaction perhaps mainly occurred in the top section of the core. In addition, living vegetation was removed before coring, and this might unintentionally remove some peat materials at the core surface, causing the age of core top perhaps a few years or even decades older than the sampling year. As described in Oppedal et al. (2018a), the core is divided into two distinct sedimentary units: a lower section Unit A (depth of 204–95 cm) composed of dense black peat, and an upper section Unit B (depth of 95–0 cm) composed of clayey peat interbedded with minerogenic materials. This lithological transition is also reflected in a range of measured sediment property data that have been presented in Oppedal et al. (2018a): loss-on-ignition (LOI), dry bulk density (DBD), elemental geochemistry (XRF core scanning), and magnetic susceptibility (Fig. 2). We conducted an additional analysis of LOI and DBD data in this study, in addition to the analysis of new proxies.

3.2. Chronology

Twelve radiocarbon dates from terrestrial plant macrofossils are available for the peat core as presented in Oppedal et al. (2018a) who constructed a preliminary age-depth model for Unit B after removing one potential outlier that would have caused an age reversal. Dating plant macrofossils in peat deposits decreased the possibility for the translocation of older carbon in dynamic landscapes (Thomas et al., 2019). In this study, we constructed a Bayesian age-depth model considering all dates for the entire core using the R package Bacon 2.4.3 with calibration datasets of SH1–2 Bomb (Hua et al., 2013) and the newly released SHCal20 (Hogg et al., 2020). We also generated an age-depth model based on linear interpolation using Clam 2.3.5 but with that potential outlier removed, in order to discuss the uncertainties in accumulation rate estimates that arise from the age-depth modeling.

3.3. Plant macrofossil analysis

Plant macrofossils were analyzed at 2-cm resolution throughout the core. Each subsample of 2 cm^3 was heated in a 5% (w/v) potassium hydroxide solution and subsequently washed through a 250-μm mesh sieve with distilled water into a Petri dish. Due to the small sample size, the purpose of macrofossil analysis is to characterize the general botanical composition of each peat sample. We only distinguished two identifiable peat components, brown mosses and monocots (including grasses and rushes) and estimated their relative volumetric abundance in percentage. All subsamples are dominated by these two macrofossil types and their proportions can vary dramatically between subsamples. For brown mosses, it was possible to identify to genus level based on the presence of identifiable leaves. Abundances of brown moss macrofossils were estimated using ordinal values ranging from 0 (absent or very rare) to 4 (abundant) (Mauquoy and Van Geel, 2007). Due to the large volume of minerogenic sediments in some samples we were not able to estimate the proportion of unidentifiable organic matter as usually done in macrofossil analysis (e.g., Barber et al., 1994; Loisel and Yu, 2013b). Additional components of the macrofossil content include other moss taxa that are present in minor amounts, including debris of *Sphagnum* cf. *fimbriatum* and *Syntrichia robusta*, seeds of rushes *Rostkovia magellanica* and *Juncus* spp., remains of cf. *Acaena* sp., chironomid head capsules, and unidentified mosses. These minor components are not included in the macrofossil diagram.

3.4. Isotope analysis of moss cellulose

When present in the samples, brown moss macrofossils were hand-picked with tweezers under a stereomicroscope for cellulose extraction and isotope analysis. We mainly collected leafless stems but in some samples leaves were still attached on stems and these macrofossils were also used for cellulose extraction. Leaf tissue has minor isotopic offsets from stems (Moschen et al., 2009; Kaislahti Tillman et al., 2010), but unlike *Sphagnum* sp. it is difficult to remove leaves from “fragile” brown moss stems. For leafless stems, identification to genus or species level was not possible, but we inferred their genus based on the co-occurring leaves that were identifiable and mainly belonged to one genus in each analyzed sample.

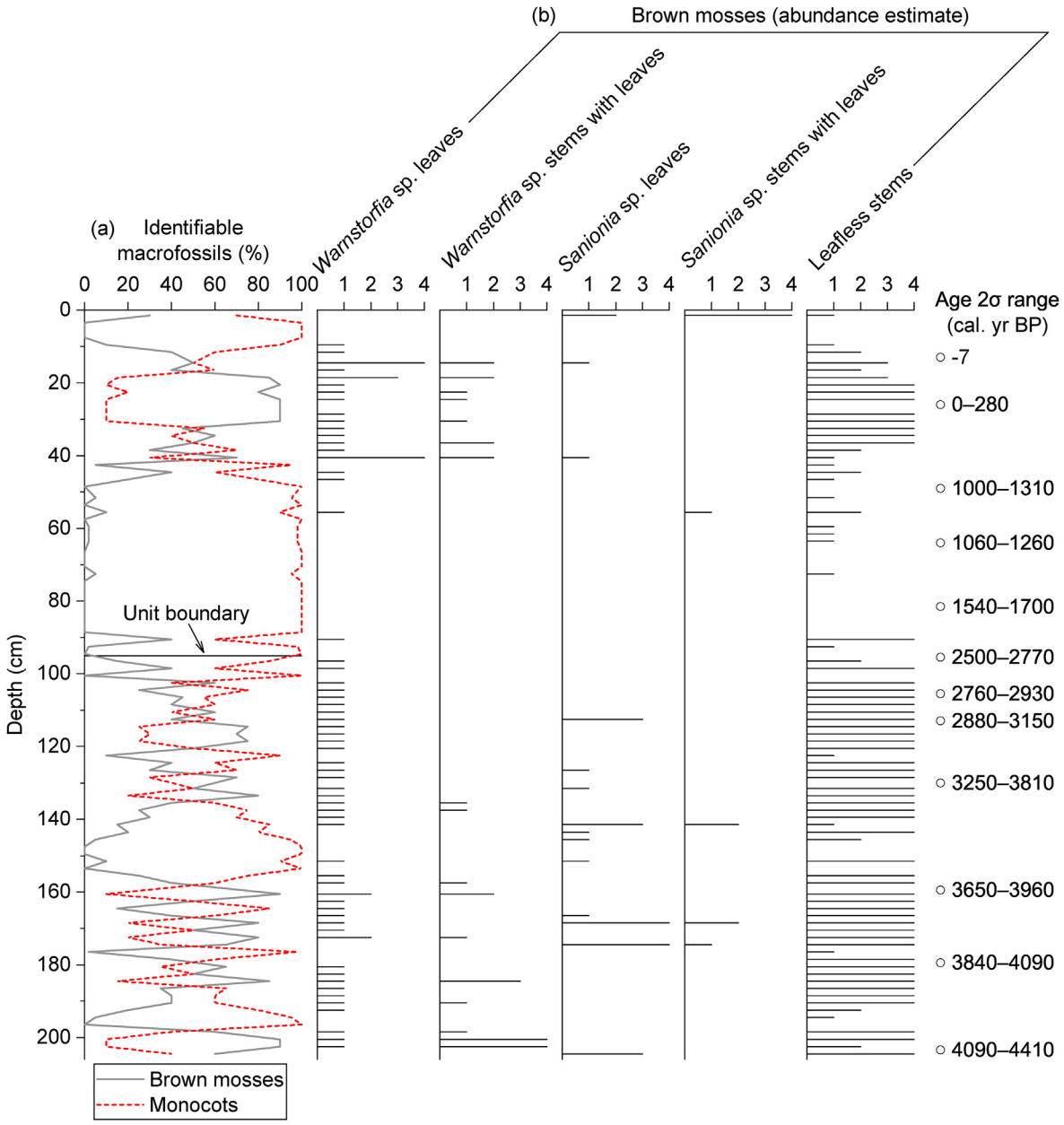

Fig. 3. Summary of plant macrofossil data for the DB2 peat core plotted versus depth. (a) Percentage in brown moss and monocot macrofossils with a horizontal line marking the transition between Units A and B. (b) Abundance estimate for different brown moss macrofossils: 0–absent or very rare, 1–occasional, 2–frequent, 3–common, 4–abundant. Calibrated calendar age range for each dating horizon is shown on the right side. The calendar age is relative to 1950 CE. (For interpretation of the references to colour in this figure legend, the reader is referred to the Web version of this article.)

The procedure for cellulose extraction followed the method developed by Kaislahti Tillman et al. (2010) but modified by Stelling and Yu (2019) for "fragile" moss species. Briefly, brown moss subsamples were transferred to disposable polypropylene columns (Poly-Prep). Samples were subjected to two rounds of 1.4% (w/v) sodium chlorite bleaching with glacial acetic acid in an 80 °C water bath for 50 min. Then samples were reacted with 10% (w/v) sodium hydroxide at 75 °C for 45 min and another round of acidified sodium chlorite bleaching. The extracted cellulose was rinsed with distilled water, transferred to vials, homogenized, and freeze-dried.

For carbon and oxygen isotope analyses, at least 0.27 mg and 0.23 mg cellulose materials were required, respectively. The extracted cellulose was enclosed in tin capsules for carbon isotope measurements and in silver capsules for oxygen isotope measurements. Carbon isotope compositions were determined on a PDZ Europa ANCA-GSL elemental analyzer interfaced to a PDZ Europa 20-20 IRMS. Oxygen isotope compositions were determined on an Elementar PyroCube interfaced to an Isoprime VisION isotope-ratio mass spectrometer (IRMS). Both isotopic analyses were carried out at the Stable Isotope Facility of the University of California, Davis. Results of isotope ratio measurements were calibrated and reported as δ notation (in per mille) referenced to VPDB (Vienna Pee Dee Belemnite) for $\delta^{13}C$ and to VSMOW (Vienna Standard Mean Ocean Water) for $\delta^{18}O$. The laboratory analytical accuracy was routinely checked, and results were corrected if necessary. The laboratory analytical precision was reported as 0.2‰ for $\delta^{13}C$ and

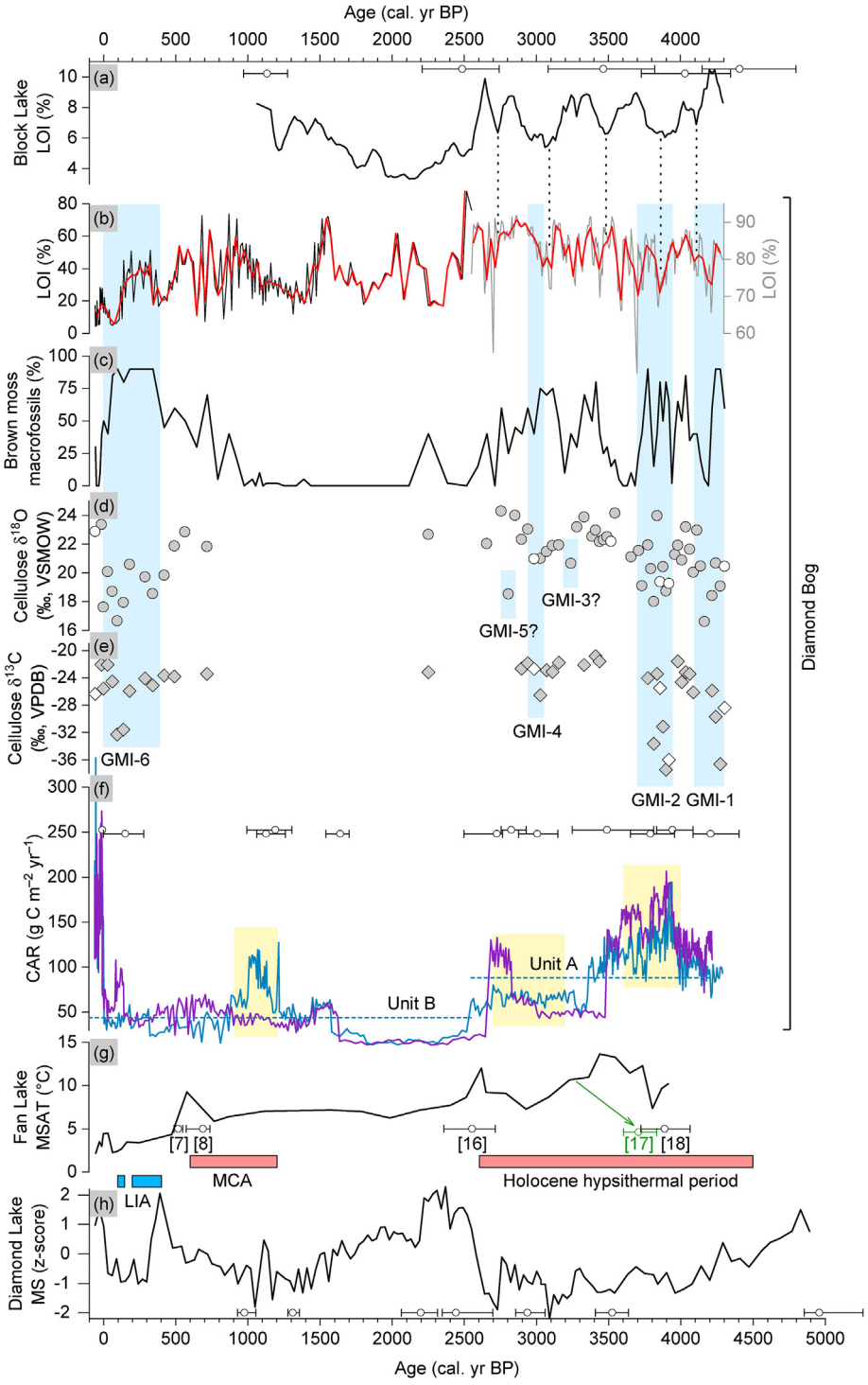

Fig. 4. Summary of proxy data from the DB2 peat core (plotted on the Bacon age-depth model) and comparisons with other regional records. For all these records, their radiocarbon dating points are also shown as dots with error bars (calibrated calendar median age with 2σ error). The calendar age is relative to 1950 CE. (a) Block Lake LOI data (5% running mean) (Rosqvist and Schuber, 2003) plotted on an updated age-depth model. (b) DB2 LOI data plotted on different vertical scales for Unit A (right vertical axis; gray line) and Unit B (left vertical axis; back line) and their 30-year bin values (red lines). The dotted lines connect the corresponding low LOI values in (a) and (b) despite a less certain chronology for the Block Lake record. (c) DB2 brown moss macrofossil percentage. (d) DB2 brown moss cellulose $\delta^{18}O$. (e) DB2 brown moss cellulose $\delta^{13}C$. In (d) and (e), gray and white symbols represent the data points from *Warnstorfia* sp. and *Sanionia* sp. macrofossils, respectively. The light blue vertical bands indicate six inferred glacial meltwater inundation (GMI) intervals. (f) DB2 "instantaneous" CARs plotted on the Bacon age-depth model (dark blue line) and the Clam age-depth model of linear interpolation (purple line). Also shown are the time-weighted mean CARs for Units A and B (dark blue horizontal dashed line) based on the Bacon age-depth model. The yellow bands indicate the observed peaks in CARs. (g) Mean summer air temperature (MSAT) record reconstructed from Fan Lake (Foster et al., 2016). Here the chronological anchor points for these temperature peaks used by Strother et al. (2015) are also shown along with their ID numbers (7, 8, 16, and 18). The green radiocarbon dating point (ID number 17) was rejected in the original age-depth model, but if used, the horizon of 3250 cal yr BP would be anchored to an older age, pulling this section of the MSAT curve rightward in the Bayesian age-depth modeling. The red horizontal bars below show the periods of past warm intervals by Foster et al. (2016) based on their multi-proxy dataset. MCA—Medieval Climate Anomaly. (h) Diamond Lake bulk magnetic susceptibility record that was used to reconstruct the size of Diamond Glacier, with a higher value indicating a larger glacier (Oppedal et al., 2018a). The blue horizontal bars above show the interval of Little Ice Age (LIA), including the peak stage at 380–220 cal yr BP and the second stage at 120 cal yr BP, defined from a well-dated high-resolution glacier-fed lake sediment record at nearby the Hamberg catchment by van der Bilt et al. (2017) (south of Fig. 1c area). (For interpretation of the references to colour in this figure legend, the reader is referred to the Web version of this article.)

0.3‰ for $\delta^{18}O$. In total, 60 samples were analyzed for $\delta^{18}O$ but only 40 samples for $\delta^{13}C$ due to insufficient cellulose materials.

3.5. Carbon accumulation rate calculation

The "instantaneous" carbon accumulation rate (CAR; g C m^{-2} yr^{-1}) for each 0.5-cm subsample (the resolution of LOI analysis; Oppedal et al., 2018a) was calculated by multiplying three metrics (Yu et al., 2014): (1) the organic matter bulk density (OMBD; g cm^{-3}) derived by multiplying DBD and LOI data, (2) the peat accumulation rate (cm yr^{-1}) derived from the age-depth model, and (3) the carbon content (% C) of organic matter, which is assumed as a constant of 51% based on the average carbon content of organic matter for non-*Sphagnum* peat (Loisel et al., 2014). Peat-core CAR reconstructions have been shown to be very sensitive to different age-depth models (Loisel et al., 2017a). Bayesian age-depth modeling has been a standard procedure to construct the peat-core chronology, but the simple linear interpolation still has an advantage in detecting the potential abrupt changes in CARs that were otherwise smoothed out in a Bayesian approach (Yu et al., 2014). We thus calculated the CARs from both the Bacon age-depth model and the Clam age-depth model of linear interpolation, and aimed to consider the uncertainties in CAR changes. We also calculated the time-weighted mean CARs for Units A and B specifically.

4. Results

The age-depth models for core DB2 are shown in Fig. 2a. Apparently, the two approaches of age-depth modeling show different results. For example, the Bacon age-depth model seems to smooth out the abrupt transition in peat accumulation rates indicated by the linear interpolation at the depth of 130 cm. Also, the potential outlier identified by Oppedal et al. (2018a) at the depth of 49 cm that would have caused an age reversal could be accommodated by the Bayesian approach. As a result, compared to the linear interpolation where this date is considered as an outlier, the horizons around the depth of 49 cm would be 250 years older in the Bacon age-depth model. Furthermore, the Bacon age-depth model produced a median age of around 4300 cal yr BP for the peat initiation and 2550 cal yr BP for the transition from Unit A to Unit B, which are 70 years older and 100 years younger than the ages from the linear interpolation, respectively (Fig. 2a). All proxy data from now on in this paper are based upon the Bacon age-depth model except for the "instantaneous" CARs that are shown on both age-depth models.

Macrofossils in Unit A are dominated by brown mosses and monocots showing frequent turnovers between these two groups of plants (Fig. 3a). Brown mosses were largely replaced by monocots after the transition into Unit B until around 1000 cal yr BP when brown mosses reappeared and subsequently disappeared again in the recent decades (Fig. 4c). The main brown moss species found are *Warnstorfia fontinaliopsis/sarmentosa*, and in a few samples *Sanionia* cf. *uncinata* (Fig. 3b). These species are known for growing in wet conditions, frequently occurring together, and forming moss carpets (Ochyra et al., 2008). Species identification for *Warnstorfia* leaves was difficult as the leaf apex was often missing.

Brown moss cellulose $\delta^{13}C$ and $\delta^{18}O$ values range from −37.5‰ to −20.9‰, and from 16.6‰ to 24.3‰, respectively (Fig. 4d and e). There are four periods with pronounced low values for cellulose $\delta^{13}C$ and $\delta^{18}O$ spanning at least a century for each: at 4300–4100, 3950–3700, 3050–2950, and 400–0 cal yr BP. In addition, there are two less prominent low cellulose $\delta^{18}O$ values at around 3250 and 2800 cal yr BP. Unfortunately, no cellulose $\delta^{13}C$ measurement is available from these intervals, due to insufficient cellulose materials from these horizons. As discussed later, these periods are interpreted as the intervals of glacial meltwater inundation (GMI), and thus we termed these six periods in chronological order as from GMI-1 to GMI-6 (Fig. 4d and e).

The LOI values range from 66% to 92% in Unit A and from 4% to 74% in Unit B, plus a few outliers (outside 1.5 interquartile ranges) presented in the box-and-whisker plot (Fig. A2a). The median LOI values for Units A and B are 83% and 29%, respectively. Due to the large range difference, LOI data are plotted on different vertical scales to better visualize the LOI changes within Unit A in Fig. 4b. There is a non-linear negative correlation in a concave shape between LOI and DBD (Fig. A2a). The median OMBD values are 0.139 g cm^{-3} for Unit A and 0.109 g cm^{-3} for Unit B (Fig. A2b). The actual OMBD values for the top section of the core are likely lower than the measured values considering the compaction of the deposits during coring. Despite this, these values are higher than that of typical *Sphagnum* peat (0.073 g cm^{-3}) and herbaceous peat (0.089 g cm^{-3}), and for Unit A the OMBD is similar to brown moss peat (0.136 g cm^{-3}) (Loisel et al., 2014). There is also a non-linear positive correlation between OMBD and LOI (Fig. A2b).

The time-weighted mean CARs for Units A and B are 88 g C m^{-2} yr^{-1} and 44 g C m^{-2} yr^{-1}, respectively (Fig. 4f). The "instantaneous" CARs have variations over an order of magnitude throughout the core. From the Bacon age-depth model (Fig. 4f), the CARs showed four periods of high values: 90–190 g C m^{-2} yr^{-1} at 4000–3500 cal yr BP, 70 g C m^{-2} yr^{-1} at 3200–2700 cal yr BP, 50–120 g C m^{-2} yr^{-1} at 1200–900 cal yr BP, and up to 250 g C m^{-2} yr^{-1} in the recent decades. The lowest CAR values of 15 g C m^{-2} yr^{-1} occurred right after the transition into Unit B, between 2500 and 1800 cal yr BP. Not surprisingly, the age offset between the two different age-depth models caused clear discrepancies in the reconstructed CARs. For example, the Clam age-depth model of linear interpolation resulted in a more dramatic peak of 120 g C m^{-2} yr^{-1} at 2800–2700 cal yr BP. This peak is "flattened" by the Bayesian approach. Also, the Clam age-depth model produced a more prolonged period of low CARs of 50 g C m^{-2} yr^{-1} occurs at 3500–3000 cal yr BP. Further, due to the removal of an age outlier, the Clam age-depth model did not produce the peak CARs at 1200–900 cal yr BP but only showed a slight increase of CARs to 60 g C m^{-2} yr^{-1} at 750–550 cal yr BP.

5. Discussion

5.1. Response of peatland carbon accumulation to the Holocene hypsithermal warmth

Unit A of core DB2 at Diamond Bog, spanning from 4300 to 2550 cal yr BP, represents a stage of stable peatland development with a vegetation cover dominated by brown mosses and monocots and with rapid carbon accumulations. High LOI values and other sediment properties suggest little minerogenic sediment influx during this period, although in the following discussion we argue that glacial meltwater pulses that have previously been overlooked still frequently affected the peatland ecosystem during this period. Magnetic susceptibility data from Diamond Lake documented a period of glacier retreat starting from 4800 cal yr BP and the Diamond Glacier remained very small between 4200 and 2700 cal yr BP (Fig. 4h) (Oppedal et al., 2018a). Similar glacier retreat was also documented in cirque glaciers from nearby the Little Jason Lagoon catchment (Berg et al., 2018) and the Block Lake catchment on the Tønsberg Peninsula (Rosqvist and Schuber, 2003) (Fig. 1c). This period was referred to as the Holocene hypsithermal period; sedimentary and paleoecological evidence for warmer climate conditions during that time was also found in the broad Antarctic

Peninsula sector (Ingólfsson et al., 1998; Hodgson et al., 2004; Bentley et al., 2009) but not clearly on the Falkland Islands north of the Antarctic Polar Front Zone (Thomas et al., 2018b). Diamond Glacier was never completely melted away during the hypsithermal period as grain size data from the Diamond Lake record still showed the presence of clay and silt produced from glacial abrasion (Oppedal et al., 2018a). This means that an overall increase in snowfall was required to replace the accelerated loss of ice due to higher temperature during this period (Dahl and Nesje, 1996). Without independent evidence, we argue that this is likely true, considering that weather station data show a robust trend in increased winter precipitation during the recent warming decades in South Georgia (Thomas et al., 2018a).

Within the hypsithermal period, the CARs have two peak periods: a major peak at 4000–3500 cal yr BP, and a second, less pronounced peak at 3200–2700 cal yr BP (Fig. 4f). The timing and structure of these two CAR peaks bear little similarity with LOI or macrofossil changes but appear to have a close correlation with regional climate. A reconstruction of summer temperature using bacterial biomarkers at nearby Fan Lake also showed two peak warmth periods at 3800–3200 and 2800–2600 cal yr BP (Fig. 4g), and this reconstruction was also supported by other proxy data in the same core (Foster et al., 2016). Fan Lake is located on Annenkov Island just southwest of the main island of South Georgia (Fig. 1b) and is on the windward side of the mountain range. Although it is in a different geographical setting from Diamond Bog, large temperature changes reconstructed from Fan Lake should reflect regional climate variability controlled by the position of the Antarctic Polar Front Zone, which might be modulated by the Southern Westerly Winds. Temperature asymmetry between windward and leeward sides of South Georgia mountain range has been observed during modern föhn events, but this effect would only cause negative and positive temperature anomalies of around 1 °C at two sides, respectively (Bannister and King, 2015). A large temperature asymmetry is unlikely under such an oceanic climate. That being said, summer temperature peaks reconstructed from Fan Lake appear to have lags of 300 years relative to the CAR peaks at Diamond Bog (Fig. 4f and g). Given that the Unit A section of the Diamond Bog peat core was well constrained by multiple radiocarbon dates and identified tephra (Oppedal et al., 2018b), we argue that these lags could be explained by a lack of radiocarbon dates in the Fan Lake sediment record during this interval, which was controlled by only two dates more than 1300 years apart (Fig. 4g). In the original age-depth model of Fan Lake, one radiocarbon date (ID number 17) within these two anchor points was rejected for the reason that the age was derived "from near tops of cores which could have been water washed or disturbed during coring" (Strother et al., 2015). If this date would have been included to adjust the original age-depth model published by Strother et al. (2015), both two temperature peaks would have been, within a Bayesian framework, about 300 years older relative to the original published age-depth model (see Fig. 4g caption). On the other hand, the chronology for the Diamond Bog peat core is still subject to the uncertainty in age-depth models, in particular for CAR reconstructions. The approach of linear age interpolation, though too simplistic, could infer changes in CARs objectively between dated intervals and could capture the rapid changes in CARs if any (Yu et al., 2014). This alternative approach would increase the second CAR peak but shorten its duration, and lengthen the duration for the transition period of low CARs in between the two peaks (Fig. 4f). The real pattern in CAR changes perhaps lies within two scenarios of age-depth models (Loisel et al., 2017a). Being aware of the uncertainties in age-depth modeling, we can still argue that the CAR changes at Diamond Bog show coincidence in magnitude and timing with temperature changes throughout the hypsithermal period. The CARs increased to as high as 140 g C m^{-2} yr^{-1} at 4000–3500 cal yr BP and 70 g C m^{-2} yr^{-1} at 3200–2700 cal yr BP when summer temperature was around 10 °C and 5 °C higher than present, respectively (Fig. 4f and g). The CARs decreased to 50 g C m^{-2} yr^{-1} during a relatively cool interval between 3350 and 3250 cal yr BP that punctuated the hypsithermal period and this cool interval was perhaps longer based on the age-depth model of linear interpolation (Fig. 4f). This interval has also been recognized in a Holocene peat sequence from Kanin Point at Husvik (Fig. 1c). At around 3400 cal yr BP, typical moss peatbank forming species (*Chorisodontium aciphyllum* and *Polytrichum strictum*) started to appear, indicating a transition to colder conditions, and then disappeared with the second peak warmth (Van der Putten et al., 2009). We caution for not overinterpreting the magnitude of temperature changes at Fan Lake and, but we suggest that the general pattern in this biomarker-based temperature record is more reliable. Although the biomarker-based paleotemperature proxy has been calibrated for modern temperature data of regional lakes, summer temperatures as high as 14 °C reconstructed from Fan Lake are outside the range of their modern calibration dataset in which the warmest site has a summer temperature of only 10 °C (Foster et al., 2016).

While the intriguing period of extreme warmth remains to be supported by additional data, the peak CARs in the Diamond Bog sequence are indeed even higher than the CARs in many recently accumulated peat deposits worldwide (Gallego-Sala et al., 2018). A global compilation of peat accumulation data has shown that for mid- and high-latitude peatlands in the northern hemisphere, their CARs are promoted by increasing temperatures that would lengthen the growing seasons and enhance the plant productivity more dramatically than enhancing the peat decomposition (MacDonald et al., 2006; Yu et al., 2009; Loisel et al., 2014; Gallego-Sala et al., 2018). We find that this direct temperature control also applied to our glacier-fed Diamond Bog that had experienced dynamic vegetation turnovers between brown mosses and monocots. That being said, it is difficult to assess whether the high CARs were also partly caused by the weaker decomposition and the better preservation of peat that would involve a range of factors and their interactions, including winter temperature, local snow cover depth and duration, glacial meltwater moistening, and summer moisture balance (Yu et al., 2009; Jones and Yu, 2010). To disentangle these factors, additional independent proxy data are needed. Previous paleoecological studies on non-glacier-fed peatlands in South Georgia suggested that relatively drier climate conditions prevailed during the hypisthermal period (Van der Putten et al., 2004, 2009). Here we assert that the overall high CARs and a sensitive response of CARs to centennial-scale warming episodes within the hypsithermal period at least suggests that Diamond Bog was rarely limited by desiccation throughout the growing seasons and was sustained by a combination of meltwater and summer precipitation inputs—the latter of which likely also increased in response to the greater vapor transport from the surrounding warmer oceans with less sea ice (Yu et al., 2009). The role of meltwater moisture supply might be more important in peat preservation and could explain why peatlands in the warmer Falkland Islands still have lower CARs at around 20 g C m^{-2} yr^{-1} than our site during the same period (Payne et al., 2019). Indeed, a study suggested that local fires have frequently occurred throughout the development of Falkland Island peatlands (Mauquoy et al., 2020).

5.2. Effect of glacial meltwater pulses during the Holocene hypsithermal period

Within Unit A, several intervals of low LOI values occurred as

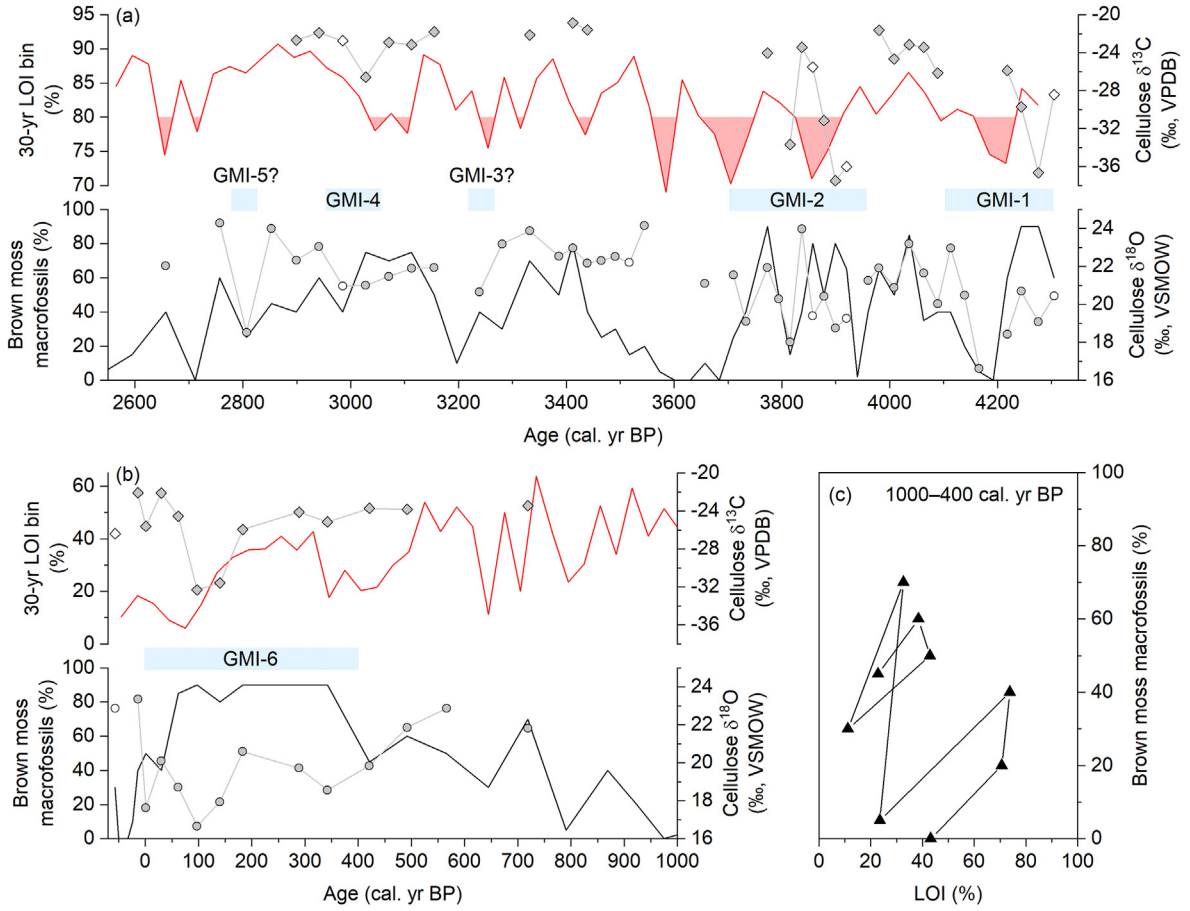

Fig. 5. A close-up view of 30-year binned LOI (red lines), brown moss macrofossil percentage (black line), and brown moss cellulose $\delta^{13}C$ and $\delta^{18}O$ (diamonds and circles) data presented in Fig. 4 for (a) Unit A and (b) the recent 1000 years in Unit B. In (a), intervals with 30-year binned LOI values lower than 80% are highlighted. Isotope data in gray and white symbols were measured from *Warnstorfia* sp. and *Sanionia* sp. macrofossils, respectively. (c) Scatter plot showing the changes in brown moss macrofossil percentage and their corresponding LOI value between 1000 and 400 cal yr BP. (For interpretation of the references to colour in this figure legend, the reader is referred to the Web version of this article.)

shown by their 30-year bin curve that averaged out the short-term variability within the glacier response time (van der Bilt et al., 2017; Oppedal et al., 2018a) (Fig. 4b). This LOI variability likely indicates small-magnitude centennial-scale changes in glacier activity, even though the overall glacier extent was reduced during the Holocene hypsithermal period. Indeed, LOI is a simple but informative metric to represent glacial sediment input in peat deposits if there was no alternative source of minerogenic sediments (Matthews et al., 2005), and this prerequisite will be briefly discussed below. We notice that in the same core the Titanium (Ti) abundance data also faithfully capture the low LOI spikes in Unit A (Fig. 2e), but magnetic susceptibility data show more low-frequency variations (Fig. 2f), suggesting more complex controlling factors (Matthews et al., 2005) such as the dissolution of magnetic minerals in acidic peat (Williams, 1992).

Aeolian transport and input of mineral particles to Diamond Bog are always possible, but from the studies of purely ombrotrophic bogs in Patagonia at the same latitude under a similar westerly flow, LOI values of more than 95% were found with little variability throughout the peat profile except major tephra layers (Xia et al., 2018; Loisel and Bunsen, 2020). Although the geomorphological context might be different as well as the source availability for aeolian transport and input, we are confident that aeolian inputs are not likely to cause the large LOI variability observed at Diamond Bog. Considering the setting of Diamond Bog, we recognize that the re-deposition of paraglacial sediments in the catchment could potentially complicate the interpretation of LOI as a proxy for glacial sediment input. In general, the Diamond Glacier catchment is small and has a short paraglacial period, and the re-deposition of paraglacial sediments during the ablation seasons would only reinforce the glacier signal in LOI (Oppedal et al., 2018a), favoring the use of LOI to represent glacier activity. That being said, we could not distinguish whether the sediments in Unit A are glacial or paraglacial origin. Another more complex mechanism is that the LOI changes are a result of the unevenness of the peatland surface, but we find that the peatland surface today is flat without any pronounced microtopography, as expected for non-*Sphagnum* peatlands (Fig. A1). Matthews et al. (2005) considered the patchy sediment deposition on the heterogeneous peatland surface as one of the major limitations of the glaciofluvial approach and suggested collecting multiple sections at the same site for such investigations. The lake record from nearby Block Lake—despite having a less certain chronology—also shows several intervals of low LOI values on the centennial-scale with coherent timing with our LOI record during this period (Fig. 4a) (Rosqvist and Schuber, 2003). This independent record from another glacierized catchment suggests that small-magnitude changes in our LOI data might reflect regional processes, but changes in glacier activity are not the sole mechanism to cause LOI variations. As such, we use LOI as a proxy for the disturbance from sediment-laden meltwater, with the

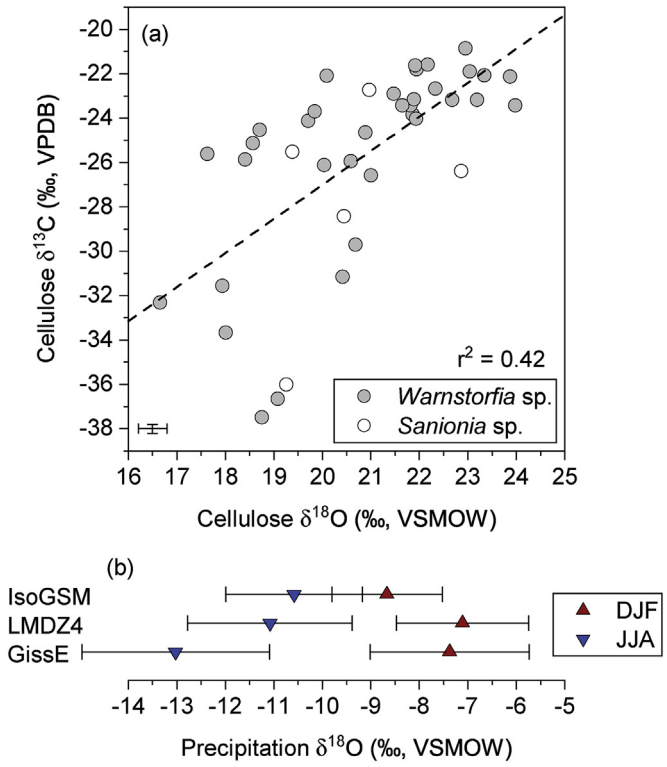

Fig. 6. (a) Scatter plot showing the positive correlation between brown moss cellulose $\delta^{13}C$ and $\delta^{18}O$. Gray and white symbols represent the data points from *Warnstorfia* sp. and *Sanionia* sp. macrofossils, respectively. The symbol in the lower left corner shows the 1σ analytical precisions for both isotope analyses. (b) The mean monthly precipitation $\delta^{18}O$ for austral summer (December–February, red triangles) and winter (June–August, blue inverted triangles) months at the location of Diamond Bog derived from three nudged isotope-enabled general circulation models for their respective reanalysis periods (Risi et al., 2012). The error bars represent the standard deviation (1σ) of monthly precipitation $\delta^{18}O$ data. (For interpretation of the references to colour in this figure legend, the reader is referred to the Web version of this article.)

strength possibly modulated by the glacier activity, to investigate their effects upon the peatland ecosystem. Finally, as will be discussed below, our moss cellulose isotope data suggest several centennial-scale meltwater inundation intervals that require persistent meltwater runoff throughout the entire growing seasons for brown mosses (not just during the snowmelt season), again favoring the glacial (rather than the snowpack) origin of sediment-laden meltwater.

A detailed look at LOI and brown moss macrofossil percentage data for Unit A shows that the brown moss vegetation on Diamond Bog was sensitive to disturbances from sediment influx. The decreases in brown moss macrofossils for the periods of 4200–4100, 3700–3500, and 3300–3200 cal yr BP, as well as at around 2700 cal yr BP, coincide with intervals of low LOI values (Fig. 5a). However, apparently not every low-LOI interval has caused a decrease in brown moss macrofossils and their link would not be captured by a linear correlation of these two time series. Also, the frequent turnovers in macrofossils between 4000 and 3750 cal yr BP seem not driven by a period of variable LOI values (Fig. 5a). These could be attributed to a complex relationship between the ecological process in vegetation turnover and the physical disturbance caused by sediment-laden meltwater. Additionally, the preservation of glacial/paraglacial sediments is, like tephra layers, affected by reworking processes in the peat matrix (Hughes et al., 2013). Therefore, there might be an inevitable mismatch between the age of peat and the exact depositional "age" of sediments in the same LOI subsample.

Stronger evidence for meltwater influence on the peatland ecosystem comes from our novel dual carbon and oxygen isotope measurements of brown moss cellulose. This is the first known coupled brown moss cellulose $\delta^{13}C$ and $\delta^{18}O$ record in peat-core studies. Although there have been quite some studies to characterize the environmental factors affecting the isotopic compositions in *Sphagnum* mosses (Aravena and Warner, 1992; Price et al., 1997; Ménot and Burns, 2001; Ménot-Combes et al., 2002; Loader et al., 2016; Granath et al., 2018; Xia et al., 2020) and their potential in peat-based paleoenvironmental reconstructions from ombrotrophic bogs (Finsinger et al., 2013; Roland et al., 2015; Xia et al., 2018), there are very few similar studies on brown moss-dominated peat systems like minerotrophic fens and those found in subantarctic and polar regions (Van der Putten et al., 2004, 2008, 2009; Loisel et al., 2017b). To confidently interpret any peat-based paleoenvironmental reconstructions, modern process understanding on brown moss cellulose $\delta^{13}C$ and $\delta^{18}O$ signals are needed. However, we propose that in our case the large ranges of cellulose $\delta^{13}C$ and $\delta^{18}O$ variations and their positive correlation throughout the studied peat core (Fig. 6a) provide direct clues on their environmental drivers.

Based on the classic "water film" mechanism for *Sphagnum* mosses, the moss cellulose $\delta^{13}C$ signal depends on the degree of diffusion resistance to plant CO_2 assimilation, with a lower cellulose $\delta^{13}C$ value corresponding to an increased discrimination against $^{13}CO_2$ under a thinner water coating on the moss leaf surface (Rice and Giles, 1996; Price et al., 1997; Loisel et al., 2010; Bramley-Alves et al., 2015). This "water film" effect should also apply to brown mosses, because of fundamentally similar physiology of bryophytes. Indeed, the majority of our measured brown moss $\delta^{13}C$ values in peat have a range from −27‰ to −21‰ (Fig. 6a), similar to what has been found in living brown mosses from dry to wet habitats on subantarctic Macquarie Island (Bramley-Alves et al., 2016) if taking into account of $\delta^{13}C$ changes in atmospheric CO_2. Several extremely low cellulose $\delta^{13}C$ observations in our data, however, are unlikely to be attributed to the "water film" effect alone, as there would be little metabolic activity once mosses were close to desiccation (Schipperges and Rydin, 1998; Royles et al., 2013), while our investigated brown moss species also prefer wet habitats (Ochyra et al., 2008). Instead, these extremely low cellulose $\delta^{13}C$ values can only be explained by a distinct non-atmospheric source of CO_2 for photosynthesis, which, in this case, would be the biogenic CH_4-derived CO_2 that is known to have very low $\delta^{13}C$ values (Raghoebarsing et al., 2005). Like *Sphagnum* mosses, brown mosses in submerged conditions could effectively develop a mutualistic symbiosis with methanotrophic bacteria that provide an additional supply of CO_2 for photosynthesis (Liebner et al., 2011). A study in the Siberian polygonal tundra showed that brown mosses in submerged habitats had much lower $\delta^{13}C$ than those in non-submerged habitats and could have $\delta^{13}C$ values as low as −33.5‰ in their bulk tissues even if these submerged brown mosses were only 10 cm below the water level (Liebner et al., 2011). In another, more detailed study in that same region, it was found that the water level and brown moss $\delta^{13}C$ did not have strong linear correlations (Zibulski et al., 2017). In particular, wet-adapted brown moss species could have large ranges of $\delta^{13}C$. We noticed that in the latter study most of their analyzed *Warnstorfia exannulata* samples—a species belonging to the same genus as in our investigated brown mosses at Diamond Bog—were collected at a water level of 0 cm (transition between submerged and non-submerged conditions) and these samples had an average $\delta^{13}C$ value of −25.7‰, ranging from −30.2‰ to −22.8‰. In only three samples collected from real submerged habitats (water level between −10

cm and 0 cm) by Zibulski et al. (2017), two of the three samples had $\delta^{13}C$ values of around −33‰, and the third one of −28.6‰. Based on this observation, we argue that the extremely low $\delta^{13}C$ values of brown mosses, as observed in their living plant data and our peat core data, could be diagnostic for the occurrence of local submerged habitat, at least for *Warnstorfia* spp.

The brown moss $\delta^{13}C$–$\delta^{18}O$ biplot indicates that these extremely low cellulose $\delta^{13}C$ values occurred with corresponding very low cellulose $\delta^{18}O$ values in the peat core (Fig. 6a). It has been well known that the moss cellulose $\delta^{18}O$ signal is determined by the source water $\delta^{18}O$ that is enriched by a biochemical enrichment factor during cellulose synthesis (Sternberg, 2009). For *Sphagnum* mosses in ombrotrophic bogs, their source water is precipitation, but evaporative enrichment of ^{18}O also occurred before that water was incorporated into cellulose synthesis (Loader et al., 2016; Xia et al., 2020). For glacier-fed peatlands such as Diamond Bog, brown mosses are hydrated by a combination of precipitation and meltwater input during their growing seasons (when temperature is higher than 0 °C; Loisel et al., 2012). Both precipitation and meltwater are considered as meteoric in origin, thus their $\delta^{18}O$ values are also controlled by macroclimate drivers such as temperature and atmospheric circulation patterns (Dansgaard, 1964). Despite this, our cellulose $\delta^{18}O$ data show high magnitude shifts to very low values over short time intervals that are unlikely to be driven by macroclimate changes (Fig. 4d). Instead, considering that changes in cellulose $\delta^{18}O$ and $\delta^{13}C$ are coupled and that the latter was interpreted as an indicator for submerged conditions for brown mosses, we infer that the drastic changes in cellulose $\delta^{18}O$ reflect the transitions between two regimes of dominant water source for moss growth: glacial meltwater and warm-season precipitation. The glacial meltwater has a "winter-like" low $\delta^{18}O$ signal as glacier ice is an archive of snowfall during the cold accumulation seasons. Diamond Glacier probably also received snowfall during the warm ablation seasons as is the case for other glaciers on South Georgia (Gordon et al., 2008). However, this effect should be minimal considering that Diamond peak is not as high as other major glaciated areas of South Georgia and that the amount of summer precipitation is less than winter precipitation in South Georgia. Summer snowfall was even less likely in warmer climate conditions during the hypsithermal period. To make peatland brown mosses—which produce most of their biomass during the warm seasons (Krebs et al., 2016; Küttim et al., 2020)—to attain such a "winter-like" low $\delta^{18}O$ signal, it would require a persistent supply of meltwater primarily from glacial ablation as their major moisture source during the growing seasons. The corresponding extremely low cellulose $\delta^{13}C$ signals suggest that this glacial meltwater also played an important role in supporting high surface wetness and submerged habitats for brown mosses. By contrast, when glacial meltwater during the ablation seasons was not the dominant supply of water, brown mosses mainly rely on intermittent precipitation events to keep hydrated and produce biomass during the warm seasons, thereby registering a "summer-like" high $\delta^{18}O$ signal in cellulose. Again, there are two endmembers of source water with distinct seasonal origins and $\delta^{18}O$ signals that dominated the source water for brown mosses over different periods. These two source water origins could shift from one to the other as shown by the rapid transitions in brown moss cellulose $\delta^{18}O$ in the Diamond Bog peat core. Although currently there are no precipitation isotope data available from South Georgia, the nudged isotope-enabled general circulation models (Risi et al., 2012) suggest that the seasonal ranges in precipitation $\delta^{18}O$ could be 2‰, 4‰, or 6‰ depending on different models (Fig. 6b). Moreover, the winter precipitation $\delta^{18}O$ at Diamond Glacier summit might be further 2‰ lower compared to that at the Diamond Bog site considering a lapse rate of 0.0065 °C/m and a precipitation $\delta^{18}O$–temperature correlation coefficient of 0.6‰ per °C (Kohn and Welker, 2005). Finally, the source water for brown mosses could be additionally affected by evaporative enrichment in ^{18}O, but less is known about whether glacial meltwater and warm-season precipitation are enriched to a different degree. If sustained pulses of glacial meltwater have a shorter residence time, we would expect a less evaporative enrichment in ^{18}O would occur and reinforce the glacial meltwater signal of relatively low $\delta^{18}O$ (Shi et al., 2019). These aforementioned factors together could justify the large contrast in $\delta^{18}O$ between two endmembers of source water.

Based on the above interpretations on cellulose isotope signatures from brown moss macrofossils, coupled abrupt and large magnitude shifts to lower cellulose $\delta^{18}O$ and $\delta^{13}C$ values could be explained by glacial meltwater inundations of the peatland. Brown moss cellulose $\delta^{18}O$ is a proxy for the proportion of source water derived from glacial meltwater during the growing seasons, while cellulose $\delta^{13}C$ would become extremely low only when submerged conditions were established persistently by meltwater. These periods with frequent inundations occurred at least three times during the hypsithermal period (GMI-1, GMI-2, and GMI-4). There are potentially two more shorter inundation intervals (GMI-3 and GMI-5) as shown by low cellulose $\delta^{18}O$ values (Fig. 4d), but, due to too little material available, we could not measure their corresponding cellulose $\delta^{13}C$ values to confirm whether or not the peat surface was submerged. These documented glacial meltwater inundations, except GMI-5, occurred when the peat deposit contained more minerogenic sediments transported by meltwater (Fig. 5a). Furthermore, although isotope data are non-continuous, a closer look at the data demonstrates that the brown moss cellulose $\delta^{18}O$ is tracking the brown moss macrofossil abundance, decreasing with lower brown moss macrofossil percentage and vice versa, even during the less confident intervals of GMI-3 and GMI-5 (Fig. 5a). This observation, along with the general agreement between LOI and brown moss macrofossil abundance data, implies that the peatland brown moss growth was not favored by the glacial meltwater influence. The brown moss species investigated in this study are rather small plants and form flat carpets. As a result, they have a limited access to sunlight when the peatland surface is covered by sediments. Peatland brown mosses often thrive on fens that compared to other wetland systems have a stable hydroperiod and a water table below the peatland surface, limiting surface transport and deposition of sediments (Mitsch and Gosselink, 2015). In boreal peatlands, brown moss macrofossils were found to increase after a wetland succession from marsh to fen environment, the latter of which had a reduced minerogenic sedimentation (Yu et al., 2013).

In summary, while Oppedal et al. (2018a) concluded that Unit A represents a period of continuous peat accumulations with little glacial meltwater influence, we suggested that the overlooked glacial meltwater pulses did affect the peatland vegetation throughout Unit A. Diamond Bog during this period can be classified, based on the dominance of *Warnstorfia* spp. and *Sanionia* spp., as a *Bog Peat A* according to Lewis-Smith (1981) and Van der Putten et al. (2012), a peat system with impeded drainage. These meltwater pulses and disturbance-driven dynamic vegetation, however, did not affect the CARs, which were strongly controlled by centennial-scale regional temperature changes. Instead, glacial meltwater, may play an important role in sustaining rapid peat accumulations by preventing desiccation and by decreasing peat decomposition during the hypsithermal period. The productivity of brown mosses is highly sensitive to moisture availability and increases sharply with sufficient moisture (Goetz and Price, 2016), although our data suggest that brown mosses do not favor the concomitant sediment disturbance on centennial timescales.

5.3. Peatland ecosystem response to climate and glacial meltwater disturbance after the hypsithermal period

Unit B of core DB2 at Diamond Bog—containing a large amount of clay and silt layers (Oppedal et al., 2018a)—represents a stage of unstable peatland conditions with slower carbon accumulations. The transition into Unit B at around 2550 cal yr BP was prominent and abrupt as shown by the LOI and other sediment property data from the Diamond Bog sequence (Fig. 2). The enhanced glaciogenic sedimentation was also documented in the sedimentary record at the downstream Diamond Lake (Fig. 4h) (Oppedal et al., 2018a). These shifts are interpreted as a phase of cooling-driven glacier advance during the post-hypsithermal period: a larger Diamond Glacier would enhance both abrasion of glacier beds and runoff of sediment-laden glacial meltwater (Bakke et al., 2010). Evidence for the post-hypsithermal cooling referred to as the Neoglacial period (Ingólfsson et al., 1998; Van der Putten et al., 2008; Bentley et al., 2009) was also found at other sites in South Georgia (Rosqvist and Schuber, 2003; Van der Putten et al., 2009; Strother et al., 2015; Foster et al., 2016; Berg et al., 2018). The Neoglacial period was possibly punctuated by a short interval of glacier retreat centered at around 1600 cal yr BP as shown in our Diamond Bog and Diamond Lake records (Fig. 4b and h) and other glacier-related records in South Georgia (Clapperton et al., 1989; Rosqvist and Schuber, 2003). In the Fan Lake sediment core, pollen data show a period of warming around 1600 cal yr BP (Strother et al., 2015), but the signal was not pronounced in the biomarker-based summer temperature record (Fig. 4g; Foster et al., 2016).

The onset of enhanced sediment-laden glacial meltwater influence on Diamond Bog at 2550 cal yr BP, as a result of the threshold shift in glacier and climate dynamics, not only changed the depositional environment but also had prolonged effects on the peatland ecosystem. Brown mosses were replaced by monocots until 1000 cal yr BP (Fig. 4c), and CARs abruptly decreased to merely 15 g C m^{-2} yr^{-1} (Fig. 4f). Notably, the short glacier retreat punctuating the Neoglacial period at 1600 cal yr BP was not detected in the macrofossil record, although CARs increased slightly to 60 g C m^{-2} yr^{-1} due to the relatively high LOI values of 60% (Fig. 4b and f). However, it is difficult to assess if the decrease in CARs during the Neoglacial period was mainly driven by the climate cooling effect on plant productivity, or the sediment deposition on the peatland surface impeding plant growth, or a combination of both. Studies have shown that, peatland carbon accumulations could either be substantially reduced or elevated after tephra depositions (Yu, 2006; Hughes et al., 2013; Ratcliffe et al., 2020) or remained stable and resilient after flooding disturbances (Hunt et al., 2013).

The re-establishment of brown moss macrofossils since 1000 cal yr BP occurred with a period of relatively high LOI values at Diamond Bog (Fig. 4b) and still low magnetic susceptibility in the Diamond Lake record (Fig. 4h), suggesting that it was likely favored by the reduced glaciogenic sedimentation. The CARs based on the Bacon age-depth model increased from 40 g C m^{-2} yr^{-1} before 1200 cal yr BP to over 100 g C m^{-2} yr^{-1} at 1200–900 cal yr BP. This brown moss re-establishment thus likely benefited from rapid peat accumulations that built up organic matter matrix and stabilized the local habitat. The period of increased CARs could also be driven by climate warming. At Fan Lake. a biomarker-based summer temperature increase of 4 °C was inferred at around 600 cal yr BP (Fig. 4g), but other multi-proxy data in the same core documented this warming period earlier and formally from 1200 to 600 cal yr BP, referred to as the regional Medieval Climate Anomaly (Foster et al., 2016). Not to mention the uncertainties in age-depth models that seem large for both cores, a comparison between two cores then would place the initial build-up of organic matter and the gradual re-establishment of brown mosses in the first and second half of this warming period, respectively.

Brown moss macrofossil abundance increased gradually since the initial re-establishment and finally became the dominant macrofossils at 350–50 cal yr BP, even though the Diamond Bog LOI decreased when brown mosses became more abundant (Fig. 5b). There is a well-documented glacier expansion episode in South Georgia referred to as the regional Little Ice Age peaking at 380–220 cal yr BP with a second, less pronounced peak at 120 cal yr BP (Fig. 4h; Roberts et al., 2010; van der Bilt et al., 2017). At Diamond Lake, there is an abrupt increase in magnetic susceptibility documenting this glacier expansion in this catchment (Fig. 4h) but with a less certain chronology (Oppedal et al., 2018a). The equilibrium-line-altitude of cirque glaciers on South Georgia was argued to have a 50-m lowering during the Little Ice Age (Clapperton et al., 1989; Oppedal et al., 2018a). The increased glacial meltwater influence and sediment influx as a result of this glacier advance should have increased disturbances for brown mosses. We find that this disturbance effect might be the case over the short-term timescales as shown by the scatter plot (Fig. 5c) in which brown moss macrofossil abundance would increase (decrease) when LOI increased (decreased) between samples, but the overall trend is opposite between 1000 and 400 cal yr BP (Fig. 5b and c). That is, brown mosses still became more abundant when glacial meltwater influence was enhanced over this period. Paired cellulose $\delta^{13}C$ and $\delta^{18}O$ data confirm that brown moss vegetation was fully developed within a glacial meltwater inundation interval (GMI-6) when brown moss macrofossils reached their peak abundance (Fig. 5b). The pattern that brown mosses became dominant with increased glacial meltwater influence is in contrast to what has been observed in Unit A. We provide two hypotheses. First, the medieval climate warming and the organic matter build-up preceding the brown moss re-establishment as well as the stabilized local habitat might have prolonged effects on the subsequent vegetation and favor the brown moss growth. Second, there might be changes in monocot taxa, such as from lawn/pool-inhabiting *Juncus* spp. to less flooding-tolerant grasses. We are currently unable to test these and other possibilities, as the ecology of peatland vegetation in South Georgia is not well documented and the taxonomic resolution of the macrofossil analysis is not high enough. This last inundation interval with brown moss dominance was eventually terminated by another major layer of glacial sediments as shown by the lowest LOI value (less than 10%) for the entire core (Fig. 4b). The peatland surface today is dry without substantial input of glacial meltwater from the small glacier and supports different vegetation from what it had several centuries ago.

The climate warming over the last century documented in weather station data likely has enhanced peat accumulations at Diamond Bog as well. However, the corresponding abrupt increase in CARs up to 250 g C m^{-2} yr^{-1} (Fig. 4f) is likely an artifact for the uncertainty in the age-depth model or because the young organic matter is less decomposed as shown by a decrease in OMBD towards the peatland surface (Fig. 2d). Similar recent increases in CARs were also documented in other peatland records in subantarctic islands and were argued to be driven by recent atmospheric circulation changes (Turney et al., 2016), but that conclusion did not take the differential decomposition history in peat deposits into consideration (Payne et al., 2019; Young et al., 2019). If a high-resolution peat-core chronology or peat accumulation data from multiple sites were available, modeling approaches could be used to correct the differential decomposition history in peat (Loisel and Yu, 2013a).

6. Conclusions

A unique multi-proxy paleoenvironmental analysis of a peat core collected from Diamond Bog on South Georgia showed that the ecosystem dynamics of this glacier-fed peatland recorded a sensitive response to climate and glacier variability. During the Holocene hypsithermal period, Diamond Glacier was too small to produce a large glacial sediment influx. As a result, the peatland vegetation was dominated by the wet-adapted brown moss species *Warnstorfia* sp. and *Sanionia* sp. that are probably less tolerant to minor sediment disturbances and were frequently replaced by monocots during several short intervals of glacial meltwater inundation. Despite the dynamic vegetation turnover during the hypsithermal period, carbon accumulation rates were sensitive to temperature changes and increased considerably during two episodes of centennial-scale climate warming. After the Holocene hypsithermal period, glacier advance as a result of climate cooling occurred abruptly, resulting in increased suspended sediment load in glacial meltwater, disrupting the brown moss vegetation that was largely replaced by monocots, and decreased carbon accumulation rates. After this transition, climate warming during the Medieval Climate Anomaly increased carbon accumulation rates again and potentially built up the organic matter matrix for the subsequent re-establishment of brown mosses. Taken together, we conclude, based on this study, that glacier-fed peatlands can be used as archives for the past glacier variability, not only based on the characteristics of their minerogenic content but also through the ecosystem responses captured in peat deposits.

Broadly speaking, our study of a glacier-fed peatland supports the notation that a warmer climate would enhance the peatland carbon sink and our data further fill the data and knowledge gaps for such mechanism on centennial timescales (Yu, 2012). The sediment-laden glacial meltwater disturbance, which strongly affects the peatland vegetation and habitat, is not a primary factor to determine the carbon accumulation rates. However, glacial meltwater pulses that provide additional water source for glacier-fed peatlands might play an important role in moistening peatlands and sustaining rapid carbon accumulations. Finally, this study for the first time shows the potential of using paired cellulose isotope measurements in brown mosses to reconstruct the paleohydrology of non-*Sphagnum* peatlands.

Author statement

J.B. and Z.Y. conceived the study. Z.X. led the new laboratory analyses. N.V.d.P. contributed to the macrofossil analysis. Z.X. and L.T.O. analyzed and interpreted the data. Z.X. wrote the manuscript. L.T.O., N.V.d.P., J.B., and Z.Y. edited the manuscript.

Declaration of competing interest

The authors declare that they have no known competing financial interests or personal relationships that could have appeared to influence the work reported in this paper.

Acknowledgements

We thank the British Antarctic Survey crew at King Edward Point and Anne Elisabeth Bjune, Åsmund Bakke, and Sunniva Solheim Vatne for help during the field work. We also thank Gunhild Rosqvist for providing updated Block Lake data, and two reviewers for helpful comments that have improved the manuscript. This study was supported by Lehigh University's College of Arts and Sciences and Department of Earth and Environmental Sciences through a summer research fellowship and a research grant to Z. Xia, and a U.S. National Science Foundation grant ERA-150289 to Z. Yu.

Appendix A. Supplementary data

Supplementary data to this article can be found online at https://doi.org/10.1016/j.quascirev.2020.106679.

References

Aravena, R., Warner, B.G., 1992. Oxygen-18 composition of *Sphagnum*, and microenvironmental water relations. Bryologist 95, 445–448. https://doi.org/10.2307/3243570.

Bakke, J., Dahl, S.O., Paasche, Ø., Riis Simonsen, J., Kvisvik, B., Bakke, K., Nesje, A., 2010. A complete record of Holocene glacier variability at Austre Okstindbreen, northern Norway: an integrated approach. Quat. Sci. Rev. 29, 1246–1262. https://doi.org/10.1016/j.quascirev.2010.02.012.

Bannister, D., King, J., 2015. Föhn winds on South Georgia and their impact on regional climate. Weather 70, 324–329. https://doi.org/10.1002/wea.2548.

Barber, K.E., Chambers, F.M., Maddy, D., Stoneman, R., Brew, J.S., 1994. A sensitive high-resolution record of late Holocene climatic change from a raised bog in northern England. Holocene 4, 198–205. https://doi.org/10.1177/095968369400400209.

Bentley, M.J., Evans, D.J.A., Fogwill, C.J., Hansom, J.D., Sugden, D.E., Kubik, P.W., 2007. Glacial geomorphology and chronology of deglaciation, South Georgia, sub-Antarctic. Quat. Sci. Rev. 26, 644–677. https://doi.org/10.1016/j.quascirev.2006.11.019.

Bentley, M.J., Hodgson, D.A., Smith, J.A., Cofaigh, C.Ó., Domack, E.W., Larter, R.D., Roberts, S.J., Brachfeld, S., Leventer, A., Hjort, C., Hillenbrand, C.-D., Evans, J., 2009. Mechanisms of Holocene palaeoenvironmental change in the Antarctic Peninsula region. Holocene 19, 51–69. https://doi.org/10.1177/0959683608096603.

Berg, S., White, D.A., Jivcov, S., Melles, M., Leng, M.J., Rethemeyer, J., Allen, C., Perren, B., Bennike, O., Viehberg, F., 2018. Holocene glacier fluctuations and environmental changes in subantarctic South Georgia inferred from a sediment record from a coastal inlet. Quat. Res. 91, 132–148. https://doi.org/10.1017/qua.2018.85.

Birnie, J., 1990. Holocene environmental change in South Georgia: evidence from lake sediments. J. Quat. Sci. 5, 171–187. https://doi.org/10.1002/jqs.3390050302.

Bramley-Alves, J., Wanek, W., French, K., Robinson, S.A., 2015. Moss $\delta^{13}C$: an accurate proxy for past water environments in polar regions. Global Change Biol. 21, 2454–2464. https://doi.org/10.1111/gcb.12848.

Bramley-Alves, J., Wanek, W., Robinson, S.A., 2016. Moss $\delta^{13}C$: implications for subantarctic palaeohydrological reconstructions. Palaeogeogr. Palaeoclimatol. Palaeoecol. 453, 20–29. https://doi.org/10.1016/j.palaeo.2016.03.028.

Clapperton, C.M., Sugden, D.E., Birnie, J., Wilson, M.J., 1989. Late-glacial and Holocene glacier fluctuations and environmental change on South Georgia, Southern Ocean. Quat. Res. 31, 210–228. https://doi.org/10.1016/0033-5894(89)90006-9.

Dahl, S.O., Nesje, A., 1996. A new approach to calculating Holocene winter precipitation by combining glacier equilibrium-line altitudes and pine-tree limits: a case study from Hardangerjokulen, central southern Norway. Holocene 6, 381–398. https://doi.org/10.1177/095968369600600401.

Dahl, S.O., Bakke, J., Lie, Ø., Nesje, A., 2003. Reconstruction of former glacier equilibrium-line altitudes based on proglacial sites: an evaluation of approaches and selection of sites. Quat. Sci. Rev. 22, 275–287. https://doi.org/10.1016/S0277-3791(02)00135-X.

Daigle, T.A., Kaufman, D.S., 2009. Holocene climate inferred from glacier extent, lake sediment and tree rings at Goat Lake, Kenai Mountains, Alaska, USA. J. Quat. Sci. 24, 33–45. https://doi.org/10.1002/jqs.1166.

Dansgaard, W., 1964. Stable isotopes in precipitation. Tellus 16, 436–468. https://doi.org/10.3402/tellusa.v16i4.8993.

Finsinger, W., Schoning, K., Hicks, S., Lücke, A., Goslar, T., Wagner-cremer, F., Hyyppä, H., 2013. Climate change during the past 1000 years: a high-temporal-resolution multiproxy record from a mire in northern Finland. J. Quat. Sci. 28, 152–164. https://doi.org/10.1002/jqs.2598.

Foster, L.C., Pearson, E.J., Juggins, S., Hodgson, D.A., Saunders, K.M., Verleyen, E., Roberts, S.J., 2016. Development of a regional glycerol dialkyl glycerol tetraether (GDGT)–temperature calibration for Antarctic and sub-Antarctic lakes. Earth Planet Sci. Lett. 433, 370–379. https://doi.org/10.1016/j.epsl.2015.11.018.

Gallego-Sala, A.V., Charman, D.J., Brewer, S., Page, S.E., Prentice, I.C., Friedlingstein, P., Moreton, S., Amesbury, M.J., Beilman, D.W., Björck, S., Blyakharchuk, T., Bochicchio, C., Booth, R.K., Bunbury, J., Camill, P., Carless, D., Chimner, R.A., Clifford, M., Cressey, E., Courtney-Mustaphi, C., De Vleeschouwer, F., de Jong, R., Fialkiewicz-Koziel, B., Finkelstein, S.A., Garneau, M., Githumbi, E., Hribjlan, J., Holmquist, J., Hughes, P.D.M., Jones, C., Jones, M.C., Karofeld, E., Klein, E.S., Kokfelt, U., Korhola, A., Lacourse, T., Le Roux, G., Lamentowicz, M., Large, D., Lavoie, M., Loisel, J., Mackay, H., MacDonald, G.M., Makila, M., Magnan, G., Marchant, R., Marcisz, K., Martínez Cortizas, A., Massa, C., Mathijssen, P., Mauquoy, D., Mighall, T., Mitchell, F.J.G., Moss, P., Nichols, J., Oksanen, P.O., Orme, L., Packalen, M.S., Robinson, S., Roland, T.P., Sanderson, N.K., Sannel, A.B.K., Silva-Sánchez, N., Steinberg, N., Swindles, G.T., Turner, T.E., Uglow, J., Väliranta, M., van Bellen, S., van der

Linden, M., van Geel, B., Wang, G., Yu, Z., Zaragoza-Castells, J., Zhao, Y., 2018. Latitudinal limits to the predicted increase of the peatland carbon sink with warming. Nat. Clim. Change 8, 907–913. https://doi.org/10.1038/s41558-018-0271-1.

Goetz, J.D., Price, J.S., 2016. Ecohydrological controls on water distribution and productivity of moss communities in western boreal peatlands, Canada. Ecohydrology 9, 138–152. https://doi.org/10.1002/eco.1620.

Gordon, J.E., Haynes, V.M., Hubbard, A., 2008. Recent glacier changes and climate trends on South Georgia. Global Planet. Change 60, 72–84. https://doi.org/10.1016/j.gloplacha.2006.07.037.

Graham, A.G.C., Kuhn, G., Meisel, O., Hillenbrand, C.-D., Hodgson, D.A., Ehrmann, W., Wacker, L., Wintersteller, P., dos Santos Ferreira, C., Römer, M., White, D., Bohrmann, G., 2017. Major advance of South Georgia glaciers during the Antarctic Cold Reversal following extensive sub-Antarctic glaciation. Nat. Commun. 8, 14798. https://doi.org/10.1038/ncomms14798.

Granath, G., Rydin, H., Baltzer, J.L., Bengtsson, F., Boncek, N., Bragazza, L., Bu, Z.J., Caporn, S.J.M., Dorrepaal, E., Galanina, O., Gałka, M., Ganeva, A., Gillikin, D.P., Goia, I., Goncharova, N., Hájek, M., Haraguchi, A., Harris, L.I., Humphreys, E., Jiroušek, M., Kajukało, K., Karofeld, E., Koronatova, N.G., Kosykh, N.P., Lamentowicz, M., Lapshina, E., Limpens, J., Linkosalmi, M., Ma, J.Z., Mauritz, M., Munir, T.M., Natali, S.M., Natcheva, R., Noskova, M., Payne, R.J., Pilkington, K., Robinson, S., Robroek, B.J.M., Rochefort, L., Singer, D., Stenøien, H.K., Tuittila, E.S., Vellak, K., Verheyden, A., Waddington, J.M., Rice, S.K., 2018. Environmental and taxonomic controls of carbon and oxygen stable isotope composition in *Sphagnum* across broad climatic and geographic ranges. Biogeosciences 15, 5189–5202. https://doi.org/10.5194/bg-15-5189-2018.

Hodgson, D.A., Doran, P.T., Roberts, D., McMinn, A., 2004. Paleolimnological studies from the Antarctic and subantarctic islands. In: Pienitz, R., Douglas, M.S.V., Smol, J.P. (Eds.), Long-term Environmental Change in Arctic and Antarctic Lakes. Springer, Dordrecht, the Netherlands, pp. 419–474.

Hogg, A.G., Heaton, T.J., Hua, Q., Palmer, J.G., Turney, C.S.M., Southon, J., Bayliss, A., Blackwell, P.G., Boswijk, G., Bronk Ramsey, C., Pearson, C., Petchey, F., Reimer, P., Reimer, R., Wacker, L., 2020. SHCal20 Southern Hemisphere calibration, 0–55,000 years cal BP. Radiocarbon 62, 759–778. https://doi.org/10.1017/RDC.2020.59.

Hua, Q., Barbetti, M., Rakowski, A.Z., 2013. Atmospheric radiocarbon for the period 1950–2010. Radiocarbon 55, 2059–2072. https://doi.org/10.2458/azu_js_rc.v55i2.16177.

Hughes, P.D.M., Mallon, G., Brown, A., Essex, H.J., Stanford, J.D., Hotes, S., 2013. The impact of high tephra loading on late-Holocene carbon accumulation and vegetation succession in peatland communities. Quat. Sci. Rev. 67, 160–175. https://doi.org/10.1016/j.quascirev.2013.01.015.

Hunt, S., Yu, Z., Jones, M., 2013. Lateglacial and Holocene climate, disturbance and permafrost peatland dynamics on the Seward Peninsula, western Alaska. Quat. Sci. Rev. 63, 42–58. https://doi.org/10.1016/j.quascirev.2012.11.019.

Ingólfsson, Ó., Hjort, C., Berkman, P.A., Björck, S., Colhoun, E., Goodwin, I.D., Hall, B., Hirakawa, K., Melles, M., Möller, P., Prentice, M.L., 1998. Antarctic glacial history since the Last Glacial Maximum: an overview of the record on land. Antarct. Sci. 10, 326–344. https://doi.org/10.1017/S095410209800039X.

Jones, M.C., Yu, Z., 2010. Rapid deglacial and early Holocene expansion of peatlands in Alaska. Proc. Natl. Acad. Sci. U.S.A. 107, 7347–7352. https://doi.org/10.1073/pnas.0911387107.

Kaislahti Tillman, P., Holzkämper, S., Kuhry, P., Sannel, A.B.K., Loader, N.J., Robertson, I., 2010. Stable carbon and oxygen isotopes in *Sphagnum fuscum* peat from subarctic Canada: implications for palaeoclimate studies. Chem. Geol. 270, 216–226. https://doi.org/10.1016/j.chemgeo.2009.12.001.

Kohn, M.J., Welker, J.M., 2005. On the temperature correlation of $\delta^{18}O$ in modern precipitation. Earth Planet Sci. Lett. 231, 87–96. https://doi.org/10.1016/j.epsl.2004.12.004.

Krebs, M., Gaudig, G., Joosten, H., 2016. Record growth of *Sphagnum papillosum* in Georgia (Transcaucasus): rain frequency, temperature and microhabitat as key drivers in natural bogs. Mires Peat 18, 1–16. https://doi.org/10.19189/MaP.2015.OMB.190.

Küttim, M., Küttim, L., Ilomets, M., Laine, A.M., 2020. Controls of *Sphagnum* growth and the role of winter. Ecol. Res. 35, 219–234. https://doi.org/10.1111/1440-1703.12074.

Lewis-Smith, R.I., 1981. Types of peat and peat-forming vegetation on South Georgia. Br. Antarct. Surv. Bull. 53, 119–139.

Liebner, S., Zeyer, J., Wagner, D., Schubert, C., Pfeiffer, E.-M., Knoblauch, C., 2011. Methane oxidation associated with submerged brown mosses reduces methane emissions from Siberian polygonal tundra. J. Ecol. 99, 914–922. https://doi.org/10.1111/j.1365-2745.2011.01823.x.

Loader, N.J., Street-Perrott, F.A., Mauquoy, D., Roland, T.P., van Bellen, S., Daley, T.J., Davies, D., Hughes, P.D.M., Pancotto, V.O., Young, G.H.F., Amesbury, M.J., Charman, D.J., Mallon, G., Yu, Z.C., 2016. Measurements of hydrogen, oxygen and carbon isotope variability in *Sphagnum* moss along a micro-topographical gradient in a southern Patagonian peatland. J. Quat. Sci. 31, 426–435. https://doi.org/10.1002/jqs.2871.

Loisel, J., Garneau, M., Hélie, J.-F., 2010. *Sphagnum* $\delta^{13}C$ values as indicators of palaeohydrological changes in a peat bog. Holocene 20, 285–291. https://doi.org/10.1177/0959683609350389.

Loisel, J., Gallego-Sala, A.V., Yu, Z., 2012. Global-scale pattern of peatland *Sphagnum* growth driven by photosynthetically active radiation and growing season length. Biogeosciences 9, 2737–2746. https://doi.org/10.5194/bg-9-2737-2012.

Loisel, J., Yu, Z., 2013a. Recent acceleration of carbon accumulation in a boreal peatland, south central Alaska. J. Geophys. Res. Biogeo. 118, 41–53. https://doi.org/10.1029/2012jg001978.

Loisel, J., Yu, Z., 2013b. Surface vegetation patterning controls carbon accumulation in peatlands. Geophys. Res. Lett. 40, 5508–5513. https://doi.org/10.1002/grl.50744.

Loisel, J., Yu, Z., Beilman, D.W., Camill, P., Alm, J., Amesbury, M.J., Anderson, D., Andersson, S., Bochicchio, C., Barber, K., Belyea, L.R., Bunbury, J., Chambers, F.M., Charman, D.J., De Vleeschouwer, F., Fiałkiewicz-Kozieł, B., Finkelstein, S.A., Gałka, M., Garneau, M., Hammarlund, D., Hinchcliffe, W., Holmquist, J., Hughes, P., Jones, M.C., Klein, E.S., Kokfelt, U., Korhola, A., Kuhry, P., Lamarre, A., Lamentowicz, M., Large, D., Lavoie, M., MacDonald, G., Magnan, G., Mäkilä, M., Mallon, G., Mathijssen, P., Mauquoy, D., McCarroll, J., Moore, T.R., Nichols, J., O'Reilly, B., Oksanen, P., Packalen, M., Peteet, D., Richard, P.J., Robinson, S., Ronkainen, T., Rundgren, M., Sannel, A.B.K., Tarnocai, C., Thom, T., Tuittila, E.-S., Turetsky, M., Väliranta, M., van der Linden, M., van Geel, B., van Bellen, S., Vitt, D., Zhao, Y., Zhou, W., 2014. A database and synthesis of northern peatland soil properties and Holocene carbon and nitrogen accumulation. Holocene 24, 1028–1042. https://doi.org/10.1177/0959683614538073.

Loisel, J., van Bellen, S., Pelletier, L., Talbot, J., Hugelius, G., Karran, D., Yu, Z., Nichols, J., Holmquist, J., 2017a. Insights and issues with estimating northern peatland carbon stocks and fluxes since the Last Glacial Maximum. Earth Sci. Rev. 165, 59–80. https://doi.org/10.1016/j.earscirev.2016.12.001.

Loisel, J., Yu, Z., Beilman, D.W., Kaiser, K., Parnikoza, I., 2017b. Peatland ecosystem processes in the maritime Antarctic during warm climates. Sci. Rep. 7, 12344. https://doi.org/10.1038/s41598-017-12479-0.

Loisel, J., Bunsen, M., 2020. Abrupt fen-bog transition across southern Patagonia: timing, causes, and impacts on carbon sequestration. Front. Ecol. Evol. 8 https://doi.org/10.3389/fevo.2020.00273.

MacDonald, G.M., Beilman, D.W., Kremenetski, K.V., Sheng, Y., Smith, L.C., Velichko, A.A., 2006. Rapid early development of circumarctic peatlands and atmospheric CH_4 and CO_2 variations. Science 314, 285–288. https://doi.org/10.1126/science.1131722.

Matthews, J.A., Berrisford, M.S., Quentin Dresser, P., Nesje, A., Olaf Dahl, S., Elisabeth Bjune, A., Bakke, J., John, H., Birks, B., Lie, Ø., Dumayne-Peaty, L., Barnett, C., 2005. Holocene glacier history of Bjørnbreen and climatic reconstruction in central Jotunheimen, Norway, based on proximal glaciofluvial stream-bank mires. Quat. Sci. Rev. 24, 67–90. https://doi.org/10.1016/j.quascirev.2004.07.003.

Matthews, J.A., Dresser, P.Q., 2008. Holocene glacier variation chronology of the Smørstabbtindan massif, Jotunheimen, southern Norway, and the recognition of century- to millennial-scale European Neoglacial Events. Holocene 18, 181–201. https://doi.org/10.1177/0959683607085608.

Mauquoy, D., Engelkes, T., Groot, M.H.M., Markesteijn, F., Oudejans, M.G., van der Plicht, J., van Geel, B., 2002. High-resolution records of late-Holocene climate change and carbon accumulation in two north-west European ombrotrophic peat bogs. Palaeogeogr. Palaeoclimatol. Palaeoecol. 186, 275–310. https://doi.org/10.1016/S0031-0182(02)00513-8.

Mauquoy, D., Van Geel, B., 2007. Mire and peat macros. In: Elias, S.A. (Ed.), Encyclopedia of Quaternary Science. Elsevier, Amsterdam, Netherlands, pp. 2315–2336.

Mauquoy, D., Payne, R.J., Babeshko, K.V., Bartlett, R., Boomer, I., Bowey, H., Evans, C.D., Ring-Hrubesh, F., Muirhead, D., O'Callaghan, M., Piotrowska, N., Rush, G., Sloan, T., Smeaton, C., Tsyganov, A.N., Mazei, Y.A., 2020. Falkland Island peatland development processes and the pervasive presence of fire. Quat. Sci. Rev. 240, 106391. https://doi.org/10.1016/j.quascirev.2020.106391.

Ménot-Combes, G., Burns, S.J., Leuenberger, M., 2002. Variations of $^{18}O/^{16}O$ in plants from temperate peat bogs (Switzerland): implications for paleoclimatic studies. Earth Planet Sci. Lett. 202, 419–434. https://doi.org/10.1016/S0012-821X(02)00794-X.

Ménot, G., Burns, S.J., 2001. Carbon isotopes in ombrogenic peat bog plants as climatic indicators: calibration from an altitudinal transect in Switzerland. Org. Geochem. 32, 233–245. https://doi.org/10.1016/S0146-6380(00)00170-4.

Mitsch, W.J., Gosselink, J.G., 2015. Wetlands, fifth ed. John Wiley & Sons, Inc., Hoboken, NJ, USA.

Moschen, R., Kühl, N., Rehberger, I., Lücke, A., 2009. Stable carbon and oxygen isotopes in sub-fossil *Sphagnum*: assessment of their applicability for palaeoclimatology. Chem. Geol. 259, 262–272. https://doi.org/10.1016/j.chemgeo.2008.11.009.

Nesje, A., Dahl, S.O., 1991a. Late Holocene glacier fluctuations in Bevringsdalen, Jostedalsbreen region, western Norway (ca 3200–1400 BP). Holocene 1, 1–7. https://doi.org/10.1177/095968369100100102.

Nesje, A., Dahl, S.O., 1991b. Holocene glacier variations of Blåisen, Hardangerjøkulen, central southern Norway. Quat. Res. 35, 25–40. https://doi.org/10.1016/0033-5894(91)90092-J.

Ochyra, R., Lewis, S., Bednarek-Ochyra, H., 2008. The Illustrated Moss Flora of Antarctica, first ed. Cambridge University Press, Cambridge, UK.

Oppedal, L.T., Bakke, J., Paasche, Ø., Werner, J.P., van der Bilt, W.G.M., 2018a. Cirque glacier on South Georgia shows centennial variability over the last 7000 years. Front. Earth Sci. 6 https://doi.org/10.3389/feart.2018.00002.

Oppedal, L.T., van der Bilt, W.G.M., Balascio, N.L., Bakke, J., 2018b. Patagonian ash on sub-Antarctic South Georgia: expanding the tephrostratigraphy of southern South America into the Atlantic sector of the Southern Ocean. J. Quat. Sci. 33, 482–486. https://doi.org/10.1002/jqs.3035.

Owen, L.A., Finkel, R.C., Barnard, P.L., Haizhou, M., Asahi, K., Caffee, M.W., Derbyshire, E., 2005. Climatic and topographic controls on the style and timing of Late Quaternary glaciation throughout Tibet and the Himalaya defined by

^{10}Be cosmogenic radionuclide surface exposure dating. Quat. Sci. Rev. 24, 1391–1411. https://doi.org/10.1016/j.quascirev.2004.10.014.
Payne, R.J., Ring-Hrubesh, F., Rush, G., Sloan, T.J., Evans, C.D., Mauquoy, D., 2019. Peatland initiation and carbon accumulation in the Falkland Islands. Quat. Sci. Rev. 212, 213–218. https://doi.org/10.1016/j.quascirev.2019.03.022.
Price, G.D., McKenzie, J.E., Pilcher, J.R., Hoper, S.T., 1997. Carbon-isotope variation in *Sphagnum* from hummock-hollow complexes: implications for Holocene climate reconstruction. Holocene 7, 229–233. https://doi.org/10.1177/095968369700700211.
Raghoebarsing, A.A., Smolders, A.J.P., Schmid, M.C., Rijpstra, W.I.C., Wolters-Arts, M., Derksen, J., Jetten, M.S.M., Schouten, S., Sinninghe Damsté, J.S., Lamers, L.P.M., Roelofs, J.G.M., Op den Camp, H.J.M., Strous, M., 2005. Methanotrophic symbionts provide carbon for photosynthesis in peat bogs. Nature 436, 1153–1156. https://doi.org/10.1038/nature03802.
Ratcliffe, J.L., Lowe, D.J., Schipper, L.A., Gehrels, M.J., French, A.D., Campbell, D.I., 2020. Rapid carbon accumulation in a peatland following Late Holocene tephra deposition, New Zealand. Quat. Sci. Rev. 246, 106505. https://doi.org/10.1016/j.quascirev.2020.106505.
Rice, S.K., Giles, L., 1996. The influence of water content and leaf anatomy on carbon isotope discrimination and photosynthesis in *Sphagnum*. Plant Cell Environ. 19, 118–124. https://doi.org/10.1111/j.1365-3040.1996.tb00233.x.
Risi, C., Noone, D., Worden, J., Frankenberg, C., Stiller, G., Kiefer, M., Funke, B., Walker, K., Bernath, P., Schneider, M., Wunch, D., Sherlock, V., Deutscher, N., Griffith, D., Wennberg, P.O., Strong, K., Smale, D., Mahieu, E., Barthlott, S., Hase, F., García, O., Notholt, J., Warneke, T., Toon, G., Sayres, D., Bony, S., Lee, J., Brown, D., Uemura, R., Sturm, C., 2012. Process-evaluation of tropospheric humidity simulated by general circulation models using water vapor isotopologues: 1. Comparison between models and observations. J. Geophys. Res. Atmos. 117, D05303. https://doi.org/10.1029/2011jd016621.
Roberts, S.J., Hodgson, D.A., Shelley, S., Royles, J., Griffiths, H.J., Deen, T.J., Thorne, M.A.S., 2010. Establishing lichenometric ages for nineteenth- and twentieth-century glacier fluctuations on South Georgia (South Atlantic). Geogr. Ann. Ser. A 92, 125–139. https://doi.org/10.1111/j.1468-0459.2010.00382.x.
Roland, T.P., Daley, T.J., Caseldine, C.J., Charman, D.J., Turney, C.S.M., Amesbury, M.J., Thompson, G.J., Woodley, E.J., 2015. The 5.2 ka climate event: evidence from stable isotope and multi-proxy palaeoecological peatland records in Ireland. Quat. Sci. Rev. 124, 209–223. https://doi.org/10.1016/j.quascirev.2015.07.026.
Rosqvist, G.C., Schuber, P., 2003. Millennial-scale climate changes on South Georgia, Southern Ocean. Quat. Res. 59, 470–475. https://doi.org/10.1016/S0033-5894(03)00036-X.
Røthe, T.O., Bakke, J., Vasskog, K., Gjerde, M., D'Andrea, W.J., Bradley, R.S., 2015. Arctic Holocene glacier fluctuations reconstructed from lake sediments at Mitrahalvøya, Spitsbergen. Quat. Sci. Rev. 109, 111–125. https://doi.org/10.1016/j.quascirev.2014.11.017.
Royles, J., Ogée, J., Wingate, L., Hodgson, D.A., Convey, P., Griffiths, H., 2013. Temporal separation between CO_2 assimilation and growth? Experimental and theoretical evidence from the desiccation-tolerant moss *Syntrichia ruralis*. New Phytol. 197, 1152–1160. https://doi.org/10.1111/nph.12114.
Schaefer, J.M., Denton, G.H., Kaplan, M., Putnam, A., Finkel, R.C., Barrell, D.J.A., Andersen, B.G., Schwartz, R., Mackintosh, A., Chinn, T., Schlüchter, C., 2009. High-frequency Holocene glacier fluctuations in New Zealand differ from the northern signature. Science 324, 622–625. https://doi.org/10.1126/science.1169312.
Schipperges, B., Rydin, H., 1998. Response of photosynthesis of *Sphagnum* species from contrasting microhabitats to tissue water content and repeated desiccation. New Phytol. 140, 677–684. https://doi.org/10.1046/j.1469-8137.1998.00311.x.
Shi, F., Rao, Z., Cao, J., Huang, C., Wu, D., Yang, W., Sun, W., 2019. Meltwater is the dominant water source controlling α-cellulose $\delta^{18}O$ in a vascular-plant-dominated alpine peatland in the Altai Mountains, Central Asia. J. Hydrol 572, 192–205. https://doi.org/10.1016/j.jhydrol.2019.02.030.
Stelling, J.M., Yu, Z., 2019. Regional climate change recorded in moss oxygen and carbon isotopes from a late Holocene peat archive in the western Antarctic Peninsula. Geosciences 9, 282. https://doi.org/10.3390/geosciences9070282.
Sternberg, L.S.L., 2009. Oxygen stable isotope ratios of tree-ring cellulose: the next phase of understanding. New Phytol. 181, 553–562. https://doi.org/10.1111/j.1469-8137.2008.02661.x.
Strother, S.L., Salzmann, U., Roberts, S.J., Hodgson, D.A., Woodward, J., Van Nieuwenhuyze, W., Verleyen, E., Vyverman, W., Moreton, S.G., 2015. Changes in Holocene climate and the intensity of Southern Hemisphere Westerly Winds based on a high-resolution palynological record from sub-Antarctic South Georgia. Holocene 25, 263–279. https://doi.org/10.1177/0959683614557576.
Thomas, Z.A., Jones, R.T., Fogwill, C.J., Hatton, J., Williams, A.N., Hogg, A., Mooney, S., Jones, P., Lister, D., Mayewski, P., Turney, C.S.M., 2018b. Evidence for increased expression of the Amundsen Sea Low over the South Atlantic during the late Holocene. Clim. Past 14, 1727–1738. https://doi.org/10.5194/cp-14-1727-2018.
Thomas, Z., Turney, C., Allan, R., Colwell, S., Kelly, G., Lister, D., Jones, P., Beswick, M., Alexander, L., Lippmann, T., Herold, N., Jones, R., 2018a. A new daily observational record from Grytviken, South Georgia: exploring twentieth-century extremes in the South Atlantic. J. Clim. 31, 1743–1755. https://doi.org/10.1175/jcli-d-17-0353.1.
Thomas, Z.A., Turney, C.S.M., Hogg, A., Williams, A.N., Fogwill, C.J., 2019. Investigating subantarctic ^{14}C ages of different peat components: site and sample selection for developing robust age models in dynamic landscapes. Radiocarbon 61, 1009–1027. https://doi.org/10.1017/RDC.2019.54.
Turney, C.S.M., Jones, R.T., Lister, D., Jones, P., Williams, A.N., Hogg, A., Thomas, Z.A., Compo, G.P., Yin, X., Fogwill, C.J., Palmer, J., Colwell, S., Allan, R., Visbeck, M., 2016. Anomalous mid-twentieth century atmospheric circulation change over the South Atlantic compared to the last 6000 years. Environ. Res. Lett. 11, 064009 https://doi.org/10.1088/1748-9326/11/6/064009.
van der Bilt, W.G.M., Bakke, J., Werner, J.P., Paasche, Ø., Rosqvist, G., Vatle, S.S., 2017. Late Holocene glacier reconstruction reveals retreat behind present limits and two-stage Little Ice Age on subantarctic South Georgia. J. Quat. Sci. 32, 888–901. https://doi.org/10.1002/jqs.2937.
Van der Putten, N., Stieperaere, H., Verbruggen, C., Ochyra, R., 2004. Holocene palaeoecology and climate history of South Georgia (sub-Antarctica) based on a macrofossil record of bryophytes and seeds. Holocene 14, 382–392. https://doi.org/10.1191/0959683604hl714rp.
Van der Putten, N., Verbruggen, C., 2005. The onset of deglaciation of Cumberland Bay and Stromness Bay, South Georgia. Antarct. Sci. 17, 29–32. https://doi.org/10.1017/S0954102005002397.
Van der Putten, N., Hébrard, J.P., Verbruggen, C., Van de Vijver, B., Disnar, J.R., Spassov, S., de Beaulieu, J.L., De Dapper, M., Keravis, D., Hus, J., Thouveny, N., Frenot, Y., 2008. An integrated palaeoenvironmental investigation of a 6200 year old peat sequence from Ile de la Possession, Iles Crozet, sub-Antarctica. Palaeogeogr. Palaeoclimatol. Palaeoecol. 270, 179–195. https://doi.org/10.1016/j.palaeo.2008.09.014.
Van der Putten, N., Verbruggen, C., Ochyra, R., Spassov, S., de Beaulieu, J.L., De Dapper, M., Hus, J., Thouveny, N., 2009. Peat bank growth, Holocene palaeoecology and climate history of South Georgia (sub-Antarctica), based on a botanical macrofossil record. Quat. Sci. Rev. 28, 65–79. https://doi.org/10.1016/j.quascirev.2008.09.023.
Van der Putten, N., Mauquoy, D., Verbruggen, C., Björck, S., 2012. Subantarctic peatlands and their potential as palaeoenvironmental and palaeoclimatic archives. Quat. Int. 268, 65–76. https://doi.org/10.1016/j.quaint.2011.07.032.
Williams, M., 1992. Evidence for the dissolution of magnetite in recent Scottish peats. Quat. Res. 37, 171–182. https://doi.org/10.1016/0033-5894(92)90080-3.
Xia, Z., Yu, Z., Loisel, J., 2018. Centennial-scale dynamics of the southern hemisphere westerly winds across the drake passage over the past two millennia. Geology 46, 855–858. https://doi.org/10.1130/G40187.1.
Xia, Z., Zheng, Y., Stelling, J.M., Loisel, J., Huang, Y., Yu, Z., 2020. Environmental controls on the carbon and water (H and O) isotopes in peatland *Sphagnum* mosses. Geochem. Cosmochim. Acta 277, 265–284. https://doi.org/10.1016/j.gca.2020.03.034.
Young, D.M., Baird, A.J., Charman, D.J., Evans, C.D., Gallego-Sala, A.V., Gill, P.J., Hughes, P.D.M., Morris, P.J., Swindles, G.T., 2019. Misinterpreting carbon accumulation rates in records from near-surface peat. Sci. Rep. 9, 17939. https://doi.org/10.1038/s41598-019-53879-8.
Yu, Z., 2006. Holocene carbon accumulation of fen peatlands in boreal western Canada: a complex ecosystem response to climate variation and disturbance. Ecosystems 9, 1278–1288. https://doi.org/10.1007/s10021-006-0174-2.
Yu, Z., Beilman, D.W., Jones, M.C., 2009. Sensitivity of northern peatland carbon dynamics to Holocene climate change. In: Baird, A.J., Belyea, L.R., Comas, X., Reeve, A., Slater, L.D. (Eds.), Carbon Cycling in Northern Peatlands (Geophysical Monograph Series 184). American Geophysical Union, Washington, DC, pp. 55–69.
Yu, Z., Loisel, J., Turetsky, M.R., Cai, S., Zhao, Y., Frolking, S., MacDonald, G.M., Bubier, J.L., 2013. Evidence for elevated emissions from high-latitude wetlands contributing to high atmospheric CH_4 concentration in the early Holocene. Global Biogeochem. Cycles 27, 131–140. https://doi.org/10.1002/gbc.20025.
Yu, Z., Vitt, D.H., Wieder, R.K., 2014. Continental fens in western Canada as effective carbon sinks during the Holocene. Holocene 24, 1090–1104. https://doi.org/10.1177/0959683614538075.
Yu, Z.C., 2012. Northern peatland carbon stocks and dynamics: a review. Biogeosciences 9, 4071–4085. https://doi.org/10.5194/bg-9-4071-2012.
Zibulski, R., Wesener, F., Wilkes, H., Plessen, B., Pestryakova, L.A., Herzschuh, U., 2017. C/N ratio, stable isotope ($\delta^{13}C$, $\delta^{15}N$), and *n*-alkane patterns of brown mosses along hydrological gradients of low-centred polygons of the Siberian Arctic. Biogeosciences 14, 1617–1630. https://doi.org/10.5194/bg-14-1617-2017.